

Ph.D Dissertation

**In-band Full-duplex
RF Front-end for Next-generation
Wireless Communication**

차세대 무선통신을 위한
동일대역 전이중통신 무선 전단부

2020. 2. 21

**Graduate School of
Jeonbuk National University**

Division of Electronics and Information Engineering

Junhyung Jeong

**In-band Full-duplex
RF Front-end for Next-generation
Wireless Communication**

차세대 무선통신을 위한
동일대역 전이중통신 무선 전단부

2020. 2. 21

**Graduate School of
Jeonbuk National University**

Division of Electronics and Information Engineering

Junhyung Jeong

**In-band Full-duplex
RF Front-end for Next-generation
Wireless Communication**

Academic Advisor: Professor Yongchae Jeong

A Dissertation Submitted In Partial Fulfillment of the
Requirements for the Degree of
Doctor of Philosophy

2019. 9. 26

**Graduate School of
Jeonbuk National University**

Division of Electronics and Information Engineering

Junhyung Jeong

**The Ph.D dissertation of Junhyung Jeong
is approved by**

Chair, Professor, Donggu Im

Jeonbuk National University

Vice Chair, Professor, Seok-Hwan Park

Jeonbuk National University

Professor, Yongchae Jeong

Jeonbuk National University

Professor, Jongsik Lim

Soonchunhyang University

Doctor, Heungjae Choi

Cardiff University

2019. 12. 20

**Graduate School of
Jeonbuk National University**

To my beloved families and friends

감사의 글

2010 년 연구실 인턴생활을 시작할 당시에는, 제가 박사과정에 진학하고 졸업까지 할 수 있을 거라고는 생각하지 못했습니다. 학부 및 석사기간 동안 연구했던 결과가 인정받아 한 편의 논문이 된다는 건 아주 귀중한 경험이었습니다. 거기에 힘입어 연구에 흥미를 느끼게 되었고, 박사과정에 진학하였습니다. 그리고 여러 귀인의 도움을 받아 이렇게 학위까지 받을 수 있게 되었습니다. 돌이켜보면, 지난 연구실에서 지난 시간 동안 조금 더 노력했다면 더 나은 결과를 보일 수 있었을 텐데, 나태함에 빠져 시간을 보낸 것 같아 후회가 됩니다. 지금부터라도 현재의 편안함에 안주하지 않고 더 나아갈 수 있도록 노력하면서 앞으로의 일생을 나아가겠습니다.

학부 시절부터 모자란 저를 석사와 박사기간동안 지도해주신 정용채 교수님, 그리고 연구년 기간 동안 바쁘신 와중에도 저를 지도해 주시고 논문을 심사해 주신 임종식 교수님, 학문적으로 새로운 분야에 관한 많은 것을 가르쳐주시고 논문을 심사해 주신 임동구 교수님, 제가 모르는 디지털 부분에서 저와 관련된 연구 정보를 가르쳐주시고 논문을 심사해 주신 박석환 교수님, 그리고 해외에서 바쁘신 와중에도 세세하게 학위 논문을 심사해 주신 최홍재 박사님께 감사드립니다.

석사 및 박사 기간 동안 연구에 저를 이끌어 주시고 연구실 생활에 관해 많은 조언을 해주신 Girdhari Chaudhary, Phirun Kim 박사님, 김수태, 김동신, 문태수, 박성두, Kolet Mok 선배님들과 학위 기간 동안 바쁜 와중에도 저를 도와준 김재연 형, 박준식, Wang Qi, 정승호, 구자건, 안보람, Phanam Pech 에게도 감사를 드립니다.

저를 낳아주신 이래로 항상 저를 위해 헌신하시고 박사 진학도 믿고 응원해 주신 부모님께도 정말 큰 감사를 드립니다. 그리고, 다른 연구실에 있으면서도 서로 도와주고 즐겁게 대학원 생활을 할 수 있게 도와준 대학원 학우분들과 순탄한 학위 과정을 도와주신 조교 선생님들께도 감사를 드립니다. 끝으로, 연구실 시작부터 끝까지 긴 시간 동안 옆에서 기쁨과 슬픔을 함께해준 수정이에게 고맙다는 말을 전합니다.

TABLE OF CONTENTS

TABLE OF CONTENTS	i
LIST OF FIGURES	iv
ABSTRACT	1
ABBREVIATIONS	3

CHAPTER 1

DISSERTATION OVERVIEW

1.1 Introduction	5
1.2 Literature Reviews	7
1.3 Dissertation Overview	10

CHAPTER 2

IN-BAND FULL-DUPELX SYSTEM

2.1 Concept of In-band Full-duplex	12
2.2 Requirements of In-band Full-duplex	14

CHPATER 3

MATHMATICAL ANALYSIS FOR SIC TECHNIQUE

3.1 SIC Analysis with Magnitude and Phase Difference	20
3.1.1 Case 1: Constant signals along with the frequency	22
3.1.2 Case 2: Two signals with magnitude and phase variations . . .	25
3.2 SIC Analysis with Group Delay Difference	31
3.3 Summary and Discussion	36

CHPATER 4

SINGLE ANTENNA

IN-BAND FULL-DUPELX RF FRONT-END

4.1 IBFD RF Front-end using Circulator	37
4.2 Analysis of Proposed IBFD RF Front-end using Circulator	40
4.3 Experimental Results of IBFD RF Front-end using Circulator . . .	44
4.4 Summary and Discussion	57

CHPATER 5

A MAGNETIC-FREE

IN-BAND FULL-DUPLEX RF FRONT-END

USING OUT-OF-PHASE BALANCING POWER SPLITTER

5.1 Magnetic-free Balanced In-band Full-duplex RF front-end . . .	58
5.2 Evaluation of Out-of-phase Balancing Power Splitter	63
5.3 Experimental Results of Balanced IBFD RF Front-end	67
5.4 Summary and Discussion	75

CHPATER 6

CONCLUSION AND FUTURE WORK

6.1 Conclusion	76
6.2 Future work.	78
REFERENCES.	80
ABSTRCAT IN KOREAN	92
CURRICULUM VITAE	94
PUBLICATIONS	97

LIST OF FIGURES

Fig. 2.1 Transmission and reception methods: (a) frequency division duplex, (b) time division duplex, and (c) in-band full-duplex 13

Fig. 2.2 In-band full-duplex self-interference cancellation requirement in WiFi system 15

Fig. 2.3 SNR in Rx with Tx leakage signals 17

Fig. 2.4 Vectors in constellation diagram of Rx. 19

Fig. 3.1 Block diagram of IBFD RF front-end. 21

Fig. 3.2 SIC characteristics of case 1: (a) SIC magnitude and (b) SIC contours according to magnitude error rate and Δp 24

Fig. 3.3 Used (a) magnitude and (b) phase responses along with frequency in case 2 27

Fig. 3.4 SIC characteristics of case 2: (a) SIC magnitude and (b) SIC contours according to $\Delta\alpha$ and normalized frequencies 29

Fig. 3.5 SIC characteristics of case 2: SIC magnitude with $\Delta p = 0.001$ rad 30

Fig. 3.6 SIC characteristics of case 2: 60 dB SIC contours according to Δp 31

Fig. 3.7 SIC characteristics: (a) SIC magnitude and (b) SIC contours according to GD_{diff} and normalized frequencies 35

Fig. 4.1 IBFD RF front-end structures: (a) conventional and (b) proposed 39

Fig. 4.2 Frequency response of leakage path and cancelation path of IBFD RF front-end structures. 40

Fig. 4.3 Signal flow paths of proposed IBFD RF front-end using circulator 41

Fig. 4.4	Through and isolation characteristics of circulator	41
Fig. 4.5	Schematics of variable (a) attenuator and (b) phase shifter	45
Fig. 4.6	Attenuation and phase deviation characteristics of variable attenuator according to forward current at 2.14 GHz.	47
Fig. 4.7	Phase variation insertion loss deviation and characteristics of variable phase shifter according to control voltage at 2.14 GHz	47
Fig. 4.8	Ideal simulation results of isolation characteristics according to return loss of antenna.	48
Fig. 4.9	Geometry of broadband high return loss antenna.	51
Fig. 4.10	(a) Structure of simulated in HFSS, (b) 3D radiation patter, (c) x - z plane radiation pattern (d) y - z plane radiation pattern	53
Fig. 4.11	Measured return losses of broadband high return loss antenna	54
Fig. 4.12	Group delay difference between S_{Rx_main} and S_{Rx_cancel}	54
Fig. 4.13	Measured Tx and Rx path Insertion losses	56
Fig. 4.14	Photograph of measured proposed IBFD RF front-end using circulator	56
Fig. 4.15	Measured Tx / Rx isolation characteristics of proposed in-band full-dupelx RF font-end using circulator	57
Fig. 5.1	Proposed magnetic-free in-band full-duplex RF front-end	59
Fig. 5.2	(a) Out-of-phase balancing power splitter and (b) reflective signal transmitter	60
Fig. 5.3	Paths of leakage Tx signal pairs in proposed magnetic-free IBFD RF front-end	62

Fig. 5.4 Schematics of (a) ring hybrid and (b) microstrip wideband balun 65

Fig. 5.5 Signal cancellation measurement set up of 0°/180° power splitter 66

Fig. 5.6 Comparison of simulation and measurement results of
0°/180° power splitter structures 66

Fig. 5.7 Photograph of the fabricated magnetic-free in-band full-duplex circuit 68

Fig. 5.8 Measured (a) insertion losses at two Tx paths
and (b) return losses at Tx and Rx ports. 69

Fig. 5.9 Measurement results of noise figure at Rx 69

Fig. 5.10 Block diagram and photograph of
antennas setup for SIC measurement 70

Fig. 5.11 Simulated radiation patterns with to d :
(a) 3D, (b) x - y plane and (b) z - y plane at 2.5 GHz 72

Fig. 5.12 Measured isolation characteristics of proposed magnetic-free
in-band full-duplex RF front-end according to d 73

ABSTRACT

In-band full-duplex RF front-end for next-generation Wireless Communication

Junhyung Jeong

Division of Electronics and Information Engineering

Jeonbuk National University

This dissertation presents novel in-band full-duplex (IBFD) RF front-end structures for the broadband 60 dB isolation characteristics between transmitter and receiver with the mathematical analysis of the self-interference cancellation (SIC) technique.

IBFD wireless communication system is a technology that can increase the data transmission efficiency of the wireless communication system compared to the conventional TDD (time-division duplex) and FDD (frequency-division duplex) system. However, since the transmission and reception are performed in the same frequency band and time, self-interference cancellation techniques are required to separate them. The classified requirements of the SIC technique are presented according to the transceiver, harmonics and noise.

Mathematical analysis shows the characteristics of the SIC technique according to the signal conditions. SIC technique is the cancellation of two signals each other. Therefore, the SIC analysis according to the magnitude,

phase difference, group delay offset, and frequency of the two signals are presented. In this analysis, the magnitude, phase difference, and group delay error range of two signals are obtained for 60 dB wideband transmitter (Tx) / receiver (Rx) isolation.

Based on the mathematical analysis, a broadband IBFD RF front-end using a circulator is proposed. Circulators of magnetic devices have the disadvantage of degrading the performances at high frequencies, but it can easily achieve 60 dB Tx / Rx isolation characteristics using the SIC technique. Therefore, it proposed a new structure used two circulators to improve the 60 dB isolation bandwidth. Simulation and measurement results using the proposed structure and antenna with high reflection characteristics are presented.

In addition, the magnetic-free IBFD RF front-end is also proposed. This architecture used a balanced power splitter with a 180° phase difference, and the physically balanced structure to realize the broadband isolation characteristics of the IBFD RF front-end. Radiation patterns according to the arrangement of the four dipole antennas and Tx / Rx isolation characteristics of the IBFD RF front-end according to the distance among the antennas are presented.

Keywords : Balanced structure, balancing power splitter, circulator, in-band full-duplex, magnetic-free, self-interference cancellation

ABBREVIATIONS

4G	4 th generation
5G	5 th generation
ADS	advanced design system
BPF	bandpass filter
BPS	balancing power splitter
BRF	band rejection filter
CL	circulator
EVM	error vector magnitude
FDD	frequency-division duplex
GD	group delay
HFSS	high frequency structure simulator
IBDF	in-band full-duplex
IF	intermediate frequency
LNA	low noise amplifier
Mag.	magnitude
MIMO	multiple input multiple output
NF	noise figure
PA	power amplifier
RST	reflective signal transmitter

Rx	receiver
SIC	self-interference cancellation
SNR	signal-to-noise ratio
TDD	time-division duplex
Tx	transmitter
WCDMA	wideband code division multiple access

CHAPTER 1

DISSERTATION OVERVIEW

1.1 Introduction

As high-quality multimedia services develop today, wireless networks are also rapidly evolving to provide these services. Early wireless networks simply required data transmission for voice wireless calls and text, but today applications such as 4K video streaming and real-time high-quality video calls are also provided by wireless communication system. Therefore, the wireless communication system requires high capacity, high-speed data transmission to cover high-quality multimedia service demand. However, in order to increase the number of users and more stably service multimedia applications, a communication technology having a higher data transmission rate than a conventional wireless communication network is required. The multiple input multiple output (MIMO) technology is one technology that can increase the data rate used in 4G (4th generation) and current 5G (5th generation) communication systems. Especially in 5G, massive MIMO technology is one of the main technologies to enhance the data rate through beam forming technology.

Another simple way to increase the data rate is increasing the service frequency bandwidth. However, over time, service providers and applications are increased, and each application is assigned a frequency band. Therefore, there is a need for a technology for increasing data rate within a limited bandwidth because it is not possible to allocate much wider bandwidth for one application. Conventional time-division duplex (TDD) and frequency-division duplex (FDD) schemes transmit and receive separately in time and frequency bands. However, In-band full-duplex technology removes the division of transmission and reception in this time and frequency band and simultaneously transmit and receive. Compared with the conventional FDD, the in-band full-duplex (IBFD) has a double frequency spectrum efficiency, because it simultaneously transmits and receives signals on the same frequency. However, as transmitter and receiver use the same frequency, some portion of strong transmitting signals is leaked to the receiver and serves as a self-interference. Although only a very small portion of transmitting signals is leaked into the receiver, these signals can seriously interfere on receiving signals due to the relatively strong transmitting signal power. Therefore, the full-duplex transceiver should eliminate this self-interference throughout the RF, baseband

and digital stages. In this paper, it analyzes and proposes a circuit for removing a self-interference at RF front-end.

1.2 Literature Review

After the practical results of the in-band full-duplex (IBFD) system^{[1]-[2]} were reported, various approaches to realize IBFD systems have been explored for wireless communication systems. Various techniques have been studied and presented to eliminate self-interference in RF, analog and digital stages^{[3]-[57]}. Some of work tried to realize a higher data rate by combining MIMO and IBFD technology^{[45]-[48]}. However, these studies are not suitable for practical wireless IBFD systems because of narrowband operating frequency and self-interference cancellation.

The required isolation between the transmitter (Tx) and receiver (Rx) for the proper operation of the IBFD system has been studied and reported in [1]. The isolation characteristic depends on the Tx output power and Tx noise floor, but a minimum of 110 dB isolation is generally required in the overall IBFD system. Particularly in the RF stage, isolation of 60 dB or more should be achieved to protect Rx circuits and ensure the normal operations of the low noise amplifier (LNA), mixer and analog-digital converter.

The self-interference cancellation (SIC) technique is mainly used in order to obtain at least 60 dB isolation between Tx and Rx in the RF stage. The SIC techniques can be classified into an antenna SIC and the RF front-end SIC. When SIC is applied to an antenna, high isolation characteristics can be easily obtained by using the proper physical structures of the antenna^{[51]-[52]}. In general, the Tx input feeding stage of the antenna is controlled, and the electromagnetic properties of the antenna are designed to cancel out Tx leakage at Rx. Another method is to arrange each Tx and Rx antennas to achieve high isolation characteristics according to the spatial electromagnetic characteristics. However, the antenna SIC needs to use a specific antenna structure and it is not suitable for an array antennas system. Moreover, more than 60 dB isolation can be obtained over the narrow frequency band.

Also, RF front-end SIC has narrowband 60 dB isolation characteristics, but it can use various kinds of antennas on the RF front-end SIC technique. Additionally, it is less susceptible to environmental influences. In the case of a SIC circuit using magnetic devices such as a circulator, it is easy to realize the Tx and Rx isolation with a single antenna structure^[51]. However, by using a magnetic circulator alone, 60 dB isolation characteristics cannot be obtained, and other supplementary signal cancellation techniques must be additionally

used. Moreover, as the operating frequency increases, the Tx and Rx isolation characteristic is degraded due to the characteristic of magnetic devices and becomes difficult to integrate with other circuits. Without magnetic devices, realizing 60 dB isolation over a wide bandwidth is difficult. [53]-[55] show the RF front-end SIC circuits without magnetic devices. These structures replaced the magnetic device with the 3 dB hybrid coupler, balun and transformer. However, these structures degrade half of Tx output power because half of the Tx output power split by the hybrid coupler, balun and transformer is used for the Tx leakage signal cancellation in the Rx. In [57], a physical balanced structure was used to enhance the isolation bandwidth. However, the 60 dB isolation characteristic bandwidth was only 60 MHz, and it had the aforementioned drawbacks due to the use of a magnetic circulator.

TABLE I
ADVANTAGES AND DISADVANTAGES OF SIC TECHNIQUES

	Advantages	Disadvantages
Antenna SIC	<ul style="list-style-type: none"> - Simple structure 	<ul style="list-style-type: none"> - Antenna usage limitation - Narrow band isolation BW - Sensitive
RF front-end SIC	<ul style="list-style-type: none"> - Free Antenna Usage - Less sensitive 	<ul style="list-style-type: none"> - Complicate structure - Narrow band isolation BW - Insertion loss

1.3 Dissertation Overview

The main purposes of this dissertation are the mathematical analysis of the signal condition for obtaining 60 dB isolation and the implementation of new IBFD RF front-end with broadband 60 dB isolation. The SIC technique is used to implement broadband IBFD RF front-end structure. Therefore, analysis of the cancellation characteristics according to the relationship between the leakage signal and cancellation signal is presented. Moreover, new structures to obtain the broadband 60 dB SIC characteristics are proposed.

The dissertation is organized as follows.

Chapter 2 describes the operation principle of the IBFD system and requirements. This chapter explained about IBFD system and compared the transmission and reception method among conventional TDD and FDD systems. Also, specific requirements for the IBDC system are presented.

Chapter 3 describes the mathematical analysis for SIC technique. It defined the signal that changes with frequency and analyzed the phenomenon that two signals cancellation each other according to the various condition. The cancellation characteristics and bandwidths are analyzed according to the magnitude, phase, and group delay variations. Accordingly, the conditions for implementing the broadband IBFD RF font-end are presented.

Chapter 4 presents a novel broadband IBFD RF front-end with the circulator. The circulator has the disadvantages of the magnetic devices described previously. Nevertheless, circulators can be achieved 60 dB Tx / Rx isolation with a relatively simple structure using SIC technology. Therefore, new structures using circulators are proposed in order to improve the 60 dB isolation bandwidth, and experimental results are presented.

Chapter 5 propose a magnetic-free IBFD RF front-end using out-of-phase balancing power splitter. To eliminate the drawbacks of the magnetic devices, a novel magnetic-free IBFD RF front-end presented. The proposed scheme enhanced the 60 dB isolation bandwidth using an out-of-phase balancing power splitter and the physical balance structure. The advantages of the proposed structure and the measurement results are presented.

Finally, in chapter 6, the conclusion is presented. The significance and contributions of the dissertation are summarized here.

CHAPTER 2

IN-BAND FULL-DUPLEX SYSTEM

This chapter presents the transmission and reception concept of the IBFD system and its advantages compared to the conventional FDD and TDD systems. In addition, the requirements and issues for practical IBFD system operation are presented.

2.1 Concept of In-band Full-duplex

Nowadays bidirectional wireless communication systems are realized with various techniques. Representative bidirectional communication techniques are TDD and FDD. As shown in Fig. 2.1, in TDD transmission and reception are repeated according to the allocated time in the same frequency band. In case of FDD, transmission and reception are performed at the same time, but different frequency bands are allocated. Thus, transmission and reception are required to be isolated either in time or in frequency bands. Therefore, the TDD method reduces the data rate because transmission and reception are performed by dividing the time. In case of FDD, the data rate is also reduced because the

transmission and reception are performed by dividing the allocated frequency bandwidth in half.

IBFD is a technique to eliminate this problem and to realize the full bidirectional communication system. As shown in Fig. 2.1 (c), IBFD performs transmission and reception at the same time and all assigned frequency bands. This method can eliminate the problem of data rate degradation due to TDD time spacing and FDD bandwidth division.

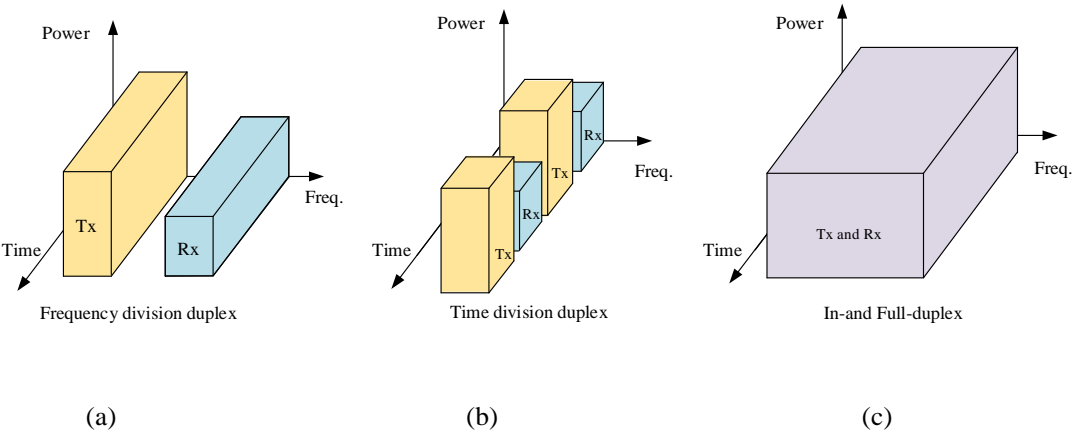


Fig. 2.1. Transmission and reception methods: (a) frequency division duplex, (b) time division duplex, and (c) in-band full-duplex.

However, conventional TDD and FDD systems separate Tx and Rx in time or frequency, whereas IBFD Tx and Rx cannot be isolated because transmission and reception are performed at the same time and frequency. Accordingly, the transmitted and received signals of Tx and Rx interfered with

each other. In the case of Tx, interference signals can be ignored because the received signal power is relatively smaller than transmitter power. On the other hand, leaked signal from Tx are much larger than Rx received signals and this leaked signal effect as an interference in Rx. This interference signal saturated or damaged the LNA and mixer in Rx and it blocks the communications. Therefore, several requirements are proposed to isolate Tx / Rx for the IBFD communication systems.

2.2 Requirements of In-band Full-duplex

The one of main requirements of an IBFD system is isolation between Tx and Rx. [1] presented the SIC requirements for the IBFD system. SIC requirements can be divided into the main Tx signal SIC (SIC_{Tx}), harmonics SIC (SIC_{Harms}), and noise SIC (SIC_{noise}). The most important SIC target is the SIC_{Tx} and it means the reduction of Tx leakage signal received at Rx. The amount of SIC requirement of operating band Tx signals is expressed as (1).

$$SIC_{Tx} \text{ (dB)} = P_{Tx} \text{ (dBm)} - NFL \text{ (dBm)} \quad (1)$$

where P_{Tx} and NFL are transmitted Tx power and noise floor level, respectively. Equation (1) shows that the amount of main signal SIC (dB) is determined by P_{Tx} and NFL of applications. For the non-distortion of the received information

at Rx, the Tx leakage signals in the Rx should be removed down to the noise floor by SIC.

Fig. 2.2 shows an example of IBFD SIC requirements in WiFi system. In the figure, SIC_{Tx} is determined to be 110 dB for P_{Tx} of 20 dBm and NFL of -90 dBm using (1). 60 dB SIC out of 110 dB is first removed from the RF stage for the normal operation of the LNA and mixer of the Rx. After RF stage SIC, the remained 50 dB SIC is obtained in the analog and digital stages to achieve the 110 dB SIC_{Tx} .

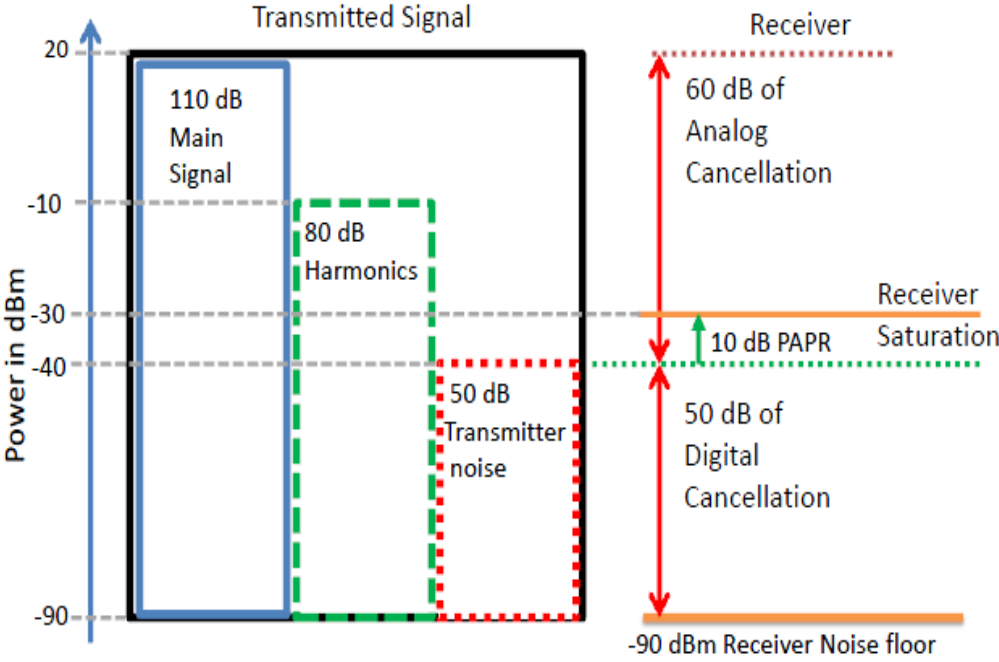


Fig. 2.2. In-band full-duplex self-interference cancellation requirement in WiFi system.

SIC_{Harms} should be removed because it affects the down conversion process in the mixer of Rx. In case of Super-Heterodyne transceiver, the IF (Intermediate frequency) band leakage signals from the Tx must be removed in Rx.

However, these SIC_{Harms} can be easily removed by a BPF (bandpass filter) or a BRF (band rejection filter) in front of the LNA, and the even-harmonics can be removed using a differential PA (power amplifier) structure and the harmonic termination PA design method.

Similarly, additional noise from Tx leaks into Rx. Therefore, this leaked noise increases the noise floor of Rx. The mathematical model cannot generate the canceling signal because the noise generated at Tx is random noise. Therefore, in general, SIC_{noise} is implemented by canceling in Rx using the noise of Tx in the analog stage.

As shown in Fig. 2.3, when all the Tx leakage signals are not canceled out at Rx, it appears as in-band noise. Eventually, this in-band noise remained in Rx degrades the signal-to-noise ratio (SNR) and EVM (error vector magnitude) performance of Rx.

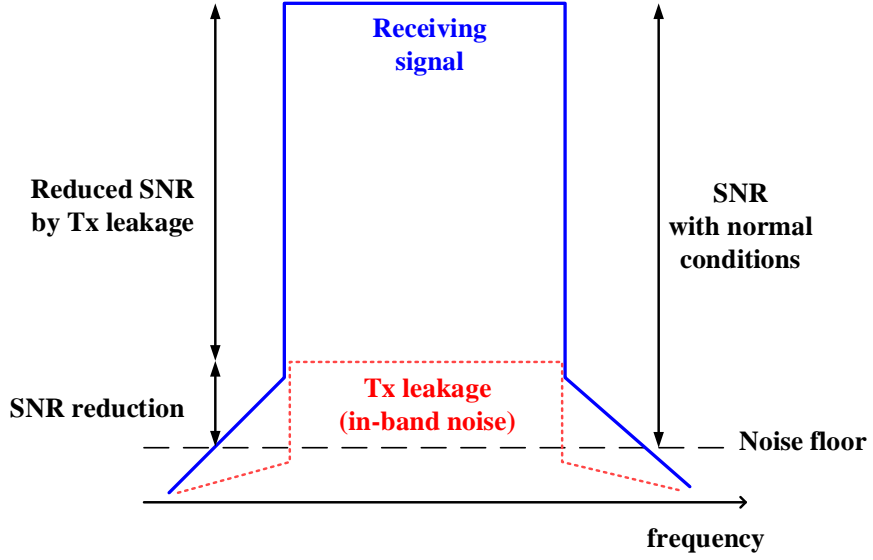


Fig. 2.3. SNR in Rx with Tx leakage signals.

Fig. 2.4 shows the vector signals in the constellation of Rx. P_{ideal} , $P_{mea.}$ and P_{error} are magnitudes of the ideal information vector, the measured vector, and the error vector, respectively. The EVM is a measure of in-band distortion of the transceiver. A signal received through the ideal transmitter and receiver have all constellation points at the ideal locations. However, self-interference in the IBFD system cause the actual constellation points to deviate from the ideal locations. The EVM of a general transceiver is expressed as (2).

$$EVM_{normal}(\%) = \frac{P_{error}}{P_{ideal}} \times 100 \quad (2)$$

EVM with only NFL error can be rewritten as in (3) when all the self-interference is removed from the IBFD system. In addition, the EVM with remaining self-interference which is larger than NFL is expressed as (4).

$$EVM_{NFL}(\%) = \frac{P_{NFL}}{P_{ideal}} \times 100 \quad (3)$$

$$EVM_{IBFD}(\%) = \frac{P_{self_inter} + P_{NFL}}{P_{ideal}} \times 100 \approx \frac{P_{self_inter}}{P_{ideal}} \times 100 \quad \left|_{P_{self_inter} \gg P_{NFL}} \quad (4)$$

where P_{self_inter} is magnitude of remained self-interference signal power in pass band. Therefore, the degradation of the EVM according to the amount of self-interference can be expressed the ratio of EVM_{NFL} and EVM_{IBFD} as

$$DG_{EVM}(\%) = \frac{EVM_{IBFD}}{EVM_{NFL}} = \frac{\frac{P_{self_inter}}{P_{ideal}}}{\frac{P_{NFL}}{P_{ideal}}} = \frac{P_{self_inter}}{P_{NFL}} \times 100 \quad (5)$$

It shows the ratio of P_{self_inter} to P_{NFL} . Therefore, when the P_{self_inter} has a lower level than the NFL , the EVM maintains the normal operation value. Otherwise, the EVM characteristic is degraded depending on the amount of the remained P_{self_inter} .

In conclusion, the main requirement of the RF stage in the IBFD system is a reduction of the main Tx leakage signal by the SIC_Tx technique. Therefore, this dissertation presents mathematical analysis and structures to remove the main Tx leakage signal up to 60 dB in broadband.

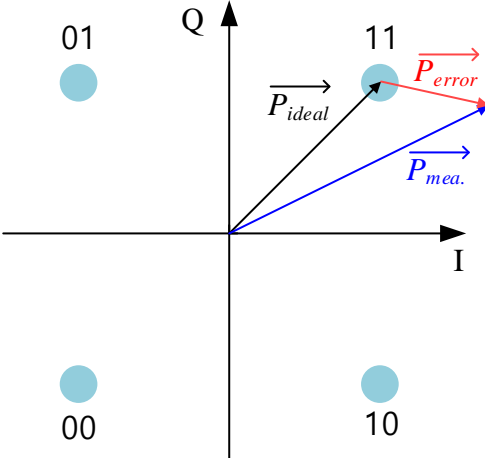


Fig. 2.4. Vectors in constellation diagram of Rx.

CHAPTER 3

MATHEMATICAL ANALYSIS FOR SIC TECHNIQUE

This section presents a mathematical analysis of the SIC technique. At first, we define the signal that varies with frequency. SIC technique means that two signals cancel each other out. Therefore, the combined signal of two signals is obtained using the defined signal. Moreover, the cancellation characteristics and bandwidths are analyzed with the signals magnitude, phase, and group delay variations. Finally, the conditions for implementing the broadband IBFD RF front-end are presented.

3.1 SIC Analysis with Magnitude and Phase Difference

At first, the signal dependence on time and frequency can be expressed as

$$\begin{aligned} S(t, f) &= Aa(f)\cos(2\pi ft + \theta(f)) \\ &= Aa(f)\{\cos(2\pi ft)\cos(\theta(f)) - \sin(2\pi ft)\sin(\theta(f))\}, \end{aligned} \quad (6)$$

where A , $a(f)$ and $\theta(f)$ are the magnitude of signal, magnitude variation function along frequency and phase variation function along frequency of the signal, respectively.

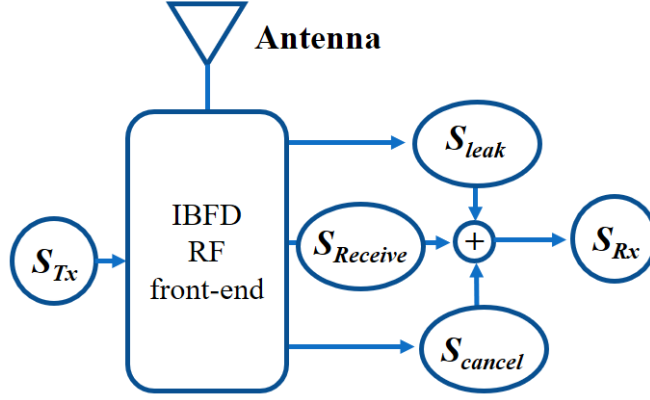


Fig. 3.1. Block diagram of IBFD RF front-end.

Fig. 3.1 shows a block diagram of IBFD RF front-end. SIC technology means that two signals cancel each other out. In IBFD, leakage signal $S_{leak}(t, f)$ and cancellation signal $S_{cancel}(t, f)$ are combined at Rx. The combined overall signal $S_{Rx}(t, f)$ in Rx can be expressed as

$$\begin{aligned}
 S_{Rx}(t, f) &= S_{leak}(t, f) + S_{cancel}(t, f) \\
 &= A_{leak} a_{leak}(f) \left\{ \cos(2\pi ft) \cos(\theta_{leak}(f)) - \sin(2\pi ft) \sin(\theta_{leak}(f)) \right\} \\
 &\quad + A_{cancel} a_{cancel}(f) \left\{ \cos(2\pi ft) \cos(\theta_{cancel}(f)) - \sin(2\pi ft) \sin(\theta_{cancel}(f)) \right\} \\
 &= \cos(2\pi ft) \left[A_{leak} a_{leak}(f) \cos(\theta_{leak}(f)) + A_{cancel} a_{cancel}(f) \cos(\theta_{cancel}(f)) \right] \\
 &\quad - \sin(2\pi ft) \left[A_{leak} a_{leak}(f) \sin(\theta_{leak}(f)) + A_{cancel} a_{cancel}(f) \sin(\theta_{cancel}(f)) \right]
 \end{aligned} \tag{7}$$

Also, the magnitude of $S_{Rx}(t, f)$ can be derived as below.

$$\begin{aligned}
 Mag_{Rx} &= |S_{Rx}(t, f)| \\
 &= \sqrt{\left[A_{leak} a_{leak}(f) \cos(\theta_{leak}(f)) + A_{cancel} a_{cancel}(f) \cos(\theta_{cancel}(f)) \right]^2 \\
 &\quad + \left[A_{leak} a_{leak}(f) \sin(\theta_{leak}(f)) + A_{cancel} a_{cancel}(f) \sin(\theta_{cancel}(f)) \right]^2}
 \end{aligned} \tag{8}$$

Now, SIC magnitude and bandwidth according to the various signal conditions are analyzed using (7) and (8).

3.1.1 Case 1: Constant signals along with the frequency

In this section, $S_{leak}(t, f)$ and $S_{cancel}(t, f)$ are assumed to have constant magnitudes A and phases φ along all frequencies. These signals mutually have a 180° phase difference to cancel out each other. In addition, the small magnitude and phase difference between two signals are as described below.

$$a_{leak}(f) = a_{cancel}(f) = 1 \quad (9a)$$

$$A_{cancel} = \Delta m + A_{leak} \quad (\Delta m : \text{magnitude difference}) \quad (9b)$$

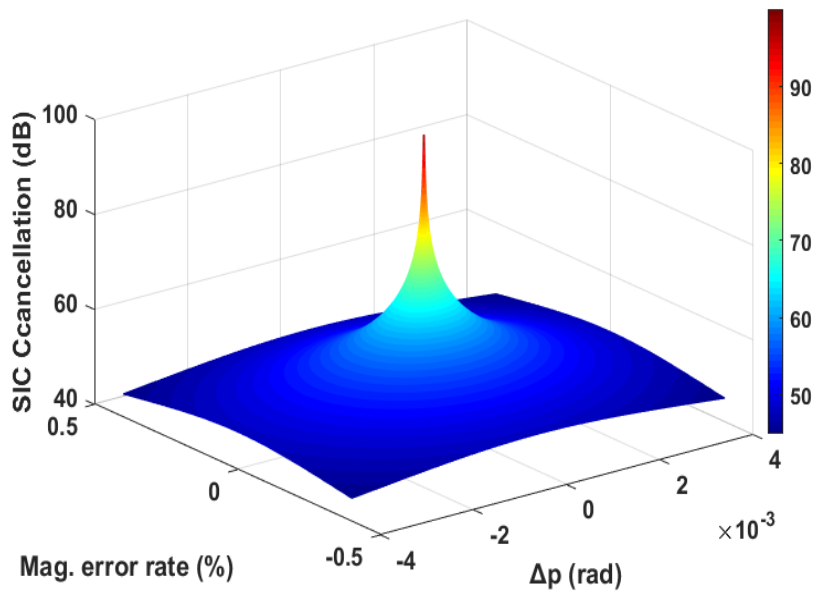
$$\theta_{leak}(f) = \varphi \quad (10a)$$

$$\theta_{cancel}(f) = \varphi + \pi + \Delta p \quad (\Delta p : \text{phase difference}) \quad (10b)$$

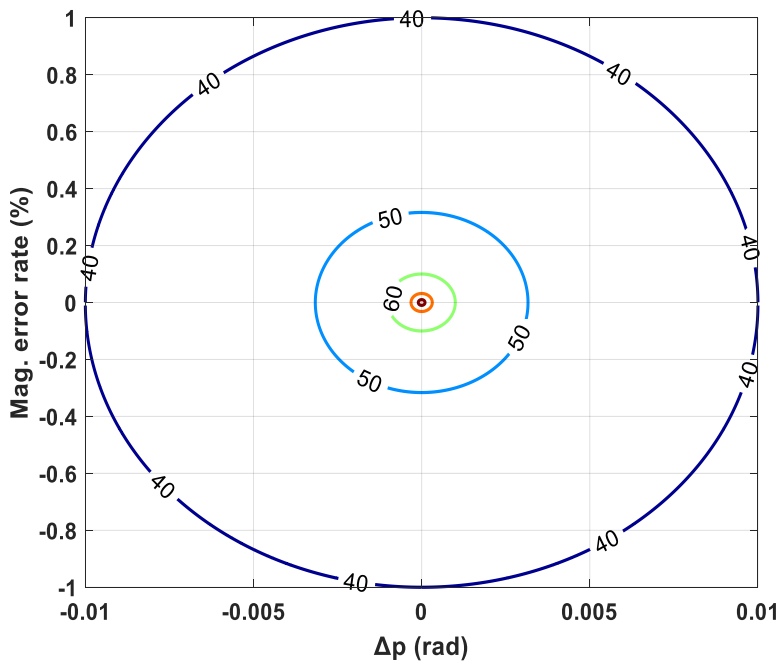
where Δm and Δp are the magnitude and phase differences between $S_{leak}(t, f)$ and $S_{cancel}(t, f)$, respectively. Using the (9) and (10), equations (7) and (8) can be developed as shown below.

$$S_{Rx_case1}(t, f) = \cos(2\pi ft) \left[A_{leak} \cos(\varphi) - (A_{leak} + \Delta m) \cos(\varphi + \Delta p) \right] \\ - \sin(2\pi ft) \left[A_{leak} \sin(\varphi) - (A_{leak} + \Delta m) \sin(\varphi + \Delta p) \right] \quad (11)$$

$$\begin{aligned}
Mag_{Rx_case1} &= \sqrt{\left[A_{leak} \cos(\varphi) - (A_{leak} + \Delta m) \cos(\varphi + \Delta p) \right]^2 \\
&\quad + \left[A_{leak} \sin(\varphi) - (A_{leak} + \Delta m) \sin(\varphi + \Delta p) \right]^2} \\
&= \sqrt{A_{leak}^2 \cos^2(\varphi) - 2A_{leak} (A_{leak} + \Delta m) \cos(\varphi) \cos(\varphi + \Delta p) \\
&\quad + (A_{leak} + \Delta m)^2 \cos^2(\varphi + \Delta p) \\
&\quad + A_{leak}^2 \sin^2(\varphi) - 2A_{leak} (A_{leak} + \Delta m) \sin(\varphi) \sin(\varphi + \Delta p) \\
&\quad + (A_{leak} + \Delta m)^2 \sin^2(\varphi + \Delta p)} \\
&= \sqrt{A_{leak}^2 + (A_{leak} + \Delta m)^2 - 2A_{leak} (A_{leak} + \Delta m) \cos(\Delta p)}. \tag{12}
\end{aligned}$$



(a)



(b)

Fig. 3.2. SIC characteristics of case 1: (a) SIC magnitude and (b) SIC contours according to magnitude error rate and Δp .

Simply, (12) shows that the SIC characteristic depends on Δm and Δp between the two constant signals. Fig. 3.1 shows the SIC magnitude in dB scale ($20\log \text{Mag}_{Rx_case1}$) using (12) with normalized A_{leak} ($A_{leak} = 1$). The magnitude (Mag.) error rate means a ratio of Δm to A ($\Delta m/A \times 100$). Fig. 3.2 (a) shows that the SIC magnitude is increased as Δm and Δp approach zero. Fig. 3.2 (b) shows the SIC contours in the range from 40 dB to 80 dB. In particular, the ranges of Mag. error rate and Δp for achieving more than 60 dB cancellation must be within $\pm 0.1\%$ and $\pm 1 \times 10^{-3}$ (± 0.001) rad, respectively. In case of 40 dB, the ranges of Mag. error rate and Δp must be within $\pm 1\%$ and ± 0.01 rad.

3.1.2 Case 2: Two signals with magnitude and phase variations

In case 1, the bandwidth cannot be analyzed because it has the same SIC characteristic for all frequencies due to the assumption of the signal does not change with frequency. Therefore, in case 2, we analyze a bandwidth according to the variation of the signal by defining a signal similar to the practical case.

Fig. 3.3 shows the magnitude and phase of the signals used in the analysis. IBFD system has the most signal leakage at the center frequency ($f_0 = 1$), and the amount of leakage decreases as it moves away from the f_0 . Therefore, $a_{leak}(f)$ and $a_{cancel}(f)$ can be expressed as (13). Fig. 3.3 (a) shows the magnitude

variation according to the magnitude slop coefficient ($\Delta\alpha$) and operating frequency variations of (13b).

$$a_{leak}(f) = 1 - \frac{(f - f_0)^2}{f_0} \quad (13a)$$

$$a_{cancel}(f) = 1 - \Delta\alpha \frac{(f - f_0)^2}{f_0} \quad (13b)$$

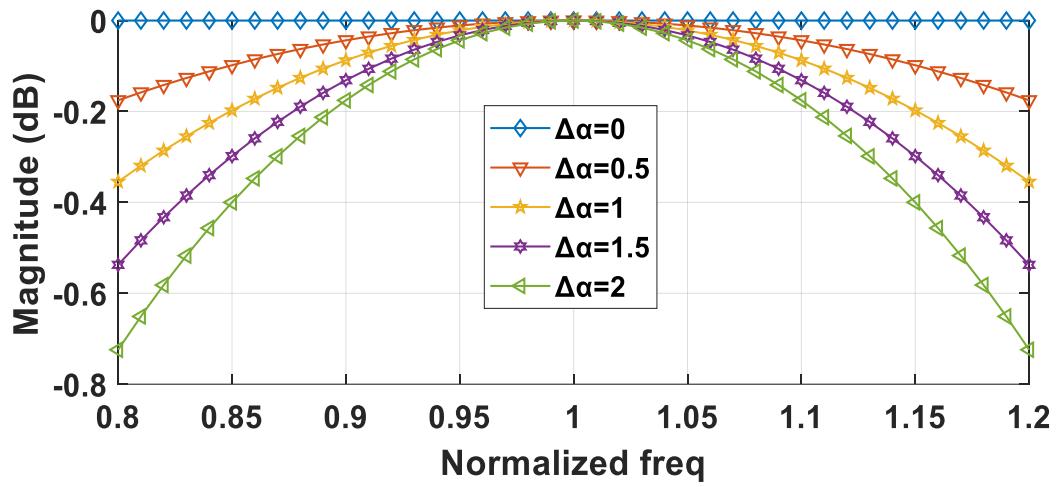
The group delay can be expressed as the phase slope of the signal in the frequency domain. In this section, we assume that the group delay of the two signals is equal. The SIC characteristics due to the group delay will be presents in Section 3.2. Therefore, the phase slope of the two leakage signals should be the same. Accordingly, the phase variations $\theta_{leak}(f)$ and $\theta_{cancel}(f)$ of the two leakage signals can be express as

$$\theta_{leak}(f) = -\frac{(f - f_0)}{f_0} - 1 \quad (14a)$$

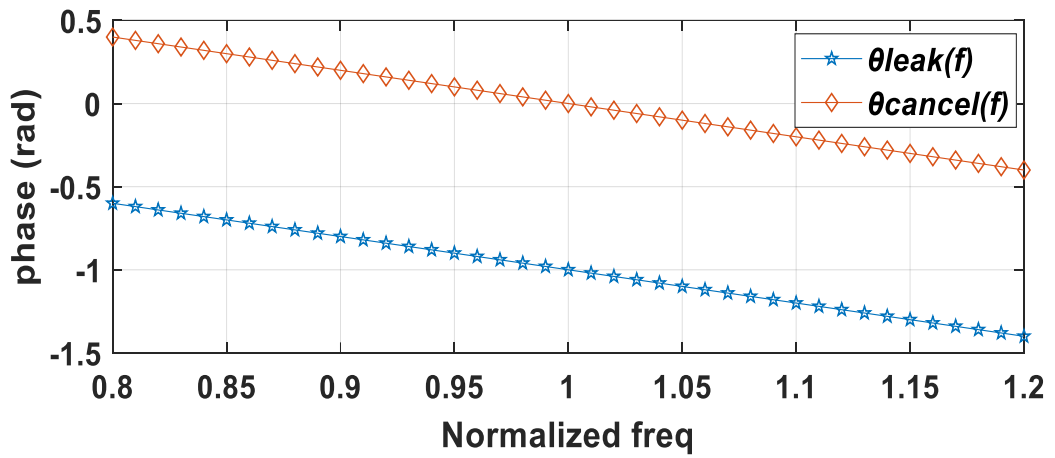
$$\theta_{cancel}(f) = -\frac{(f - f_0)}{f_0} - 1 + \Delta p \quad (14b)$$

These are the same and the phase difference between the two signals is expressed as Δp as shown in Fig. 3.3 (b). Using these conditions, (8) is substituted as

$$Mag_{Rx_case2} = \sqrt{A_{leak}^2 a_{leak}^2(f) + a_{cancel}^2(f) (\Delta m + A_{leak})^2 - 2A_{leak} (\Delta m + A_{leak}) a_{leak}(f) a_{cancel}(f) \cos(\Delta p)} \quad (15)$$



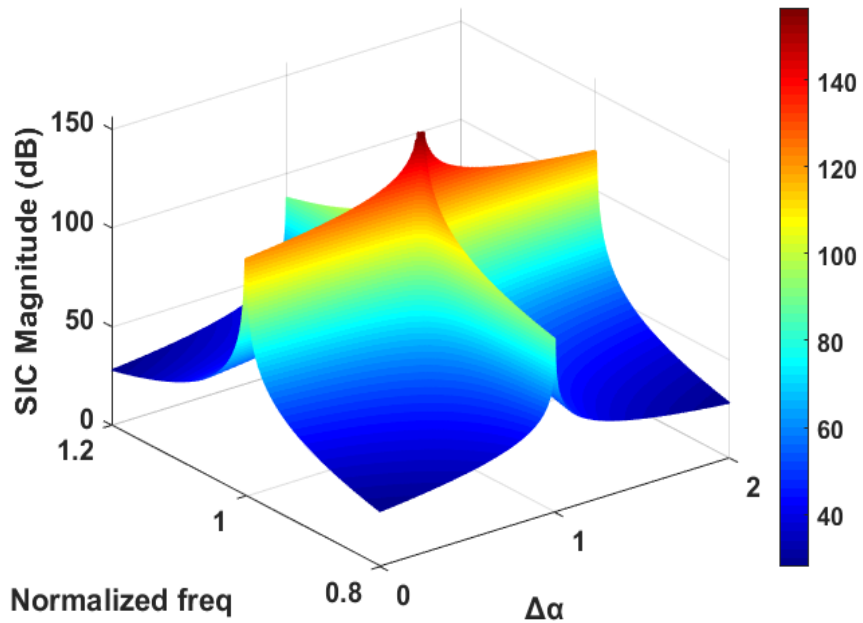
(a)



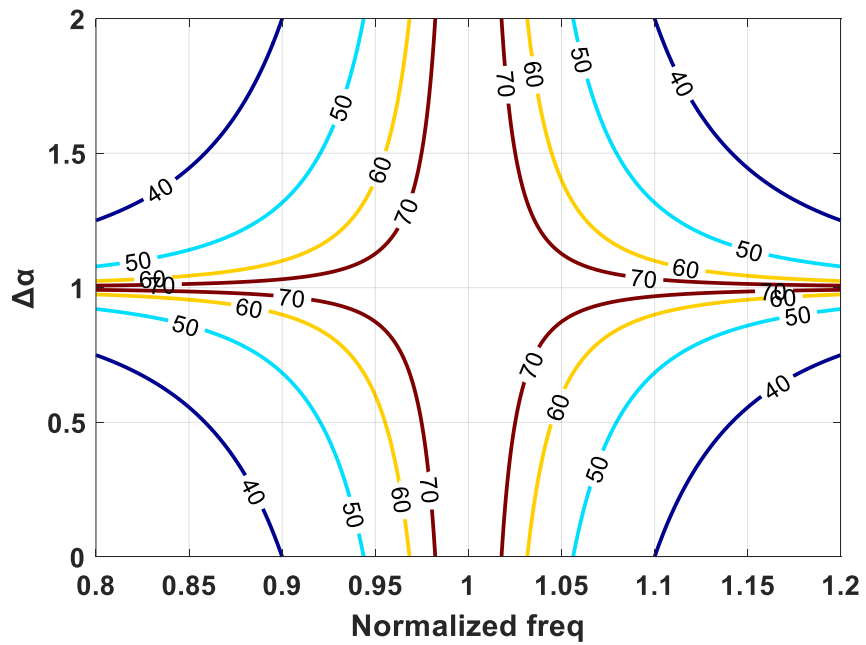
(b)

Fig. 3.3. Used (a) magnitude and (b) phase responses along with frequency in case 2.

Fig. 3.4 shows the SIC magnitude of case 2 according to normalized frequencies and $\Delta\alpha$ using (13), (14) and (15). In order to observe the tendency of SIC according to $\Delta\alpha$, the other parameters (Δm and Δp) are set to zero, except for $A_{leak} = 1$. Fig. 3.4 (a) shows that the SIC magnitude is increased as $\Delta\alpha$ approaches 1 and the operating frequency approaches f_0 because the slope constant of $a_{leak}(f)$ is 1. Fig. 3.4 (b) shows the SIC contours according to $\Delta\alpha$ and normalized frequencies. It shows that the 60 dB SIC magnitude bandwidth is reduced according to increment and decrement of the $\Delta\alpha$ from 1.



(a)



(b)

Fig. 3.4. SIC characteristics of case 2: (a) SIC magnitude and (b) SIC contours according to $\Delta\alpha$ and normalized frequencies

Fig. 3.5 shows the variation of SIC magnitude and 60 dB bandwidth according to $\Delta\alpha$, normalized frequencies with $\Delta p = 0.001$ rad. In case 1, more than 60 dB SIC can be obtained when $|\Delta p|$ is less than 0.001 rad. Therefore, Fig. 3.5 shows that the maximum SIC is 60 dB with $\Delta p = 0.001$ rad.

Fig. 3.6 shows the 60 dB SIC contours according to Δp variations with the $\Delta m = 0$ and $A_{leak} = 1$. The color-filled regions inside the traces mean more than 60 dB SIC frequencies. The 60 dB SIC frequency bandwidths at $\Delta\alpha = 1.5$ are 0.93 ~ 1.07 (14%), 0.95 ~ 1.05 (10%), and 0.99 ~ 1.01 (2%) when Δp is 0, 0.0009, and 0.001 rad, respectively. It can be observed that the 60 dB SIC bandwidth is decreased as Δp increases.

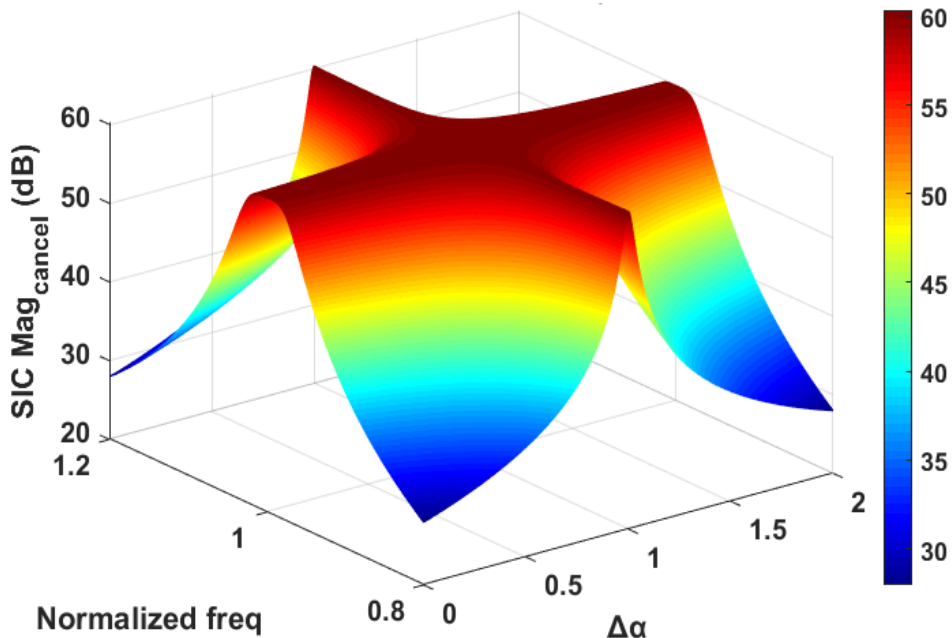


Fig. 3.5. SIC characteristics of case 2: SIC magnitude with $\Delta p = 0.001$ rad.

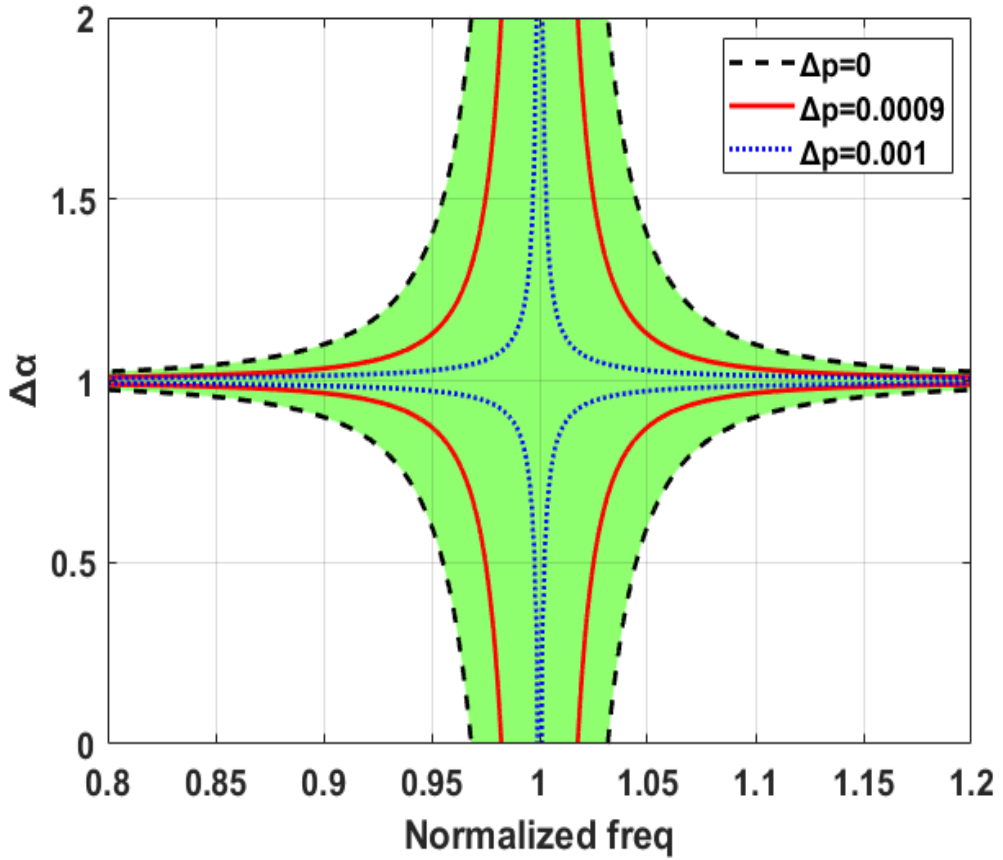


Fig. 3.6. SIC characteristics of case 2: 60 dB SIC contours according to Δp .

3.2 SIC Analysis with Group delay Difference

In the previous section, the SIC magnitude and bandwidth was analyzed according to the magnitude/phase difference and frequency variations of two signals under group delay (GD) matched condition. However, general microwave circuits have a group delay difference depending on the physical

length and electrical characteristics of each path. In this section, we analyze the SIC characteristics and bandwidth according to the group delay difference purely under the matched magnitude and phase condition. For that, the parameters except group delay are redefined as

$$a_{leak}(f) = a_{cancel}(f) = 1 \quad (16)$$

$$A_{cancel} = A_{leak} = 1 \quad (17)$$

$$\theta_{leak}(f) = -\frac{(f - f_0)}{f_0} \quad (18)$$

$$\theta_{cancel}(f) = -\Delta\beta \frac{(f - f_0)}{f_0} + \pi \quad (19)$$

where $\Delta\beta$ is phase slop coefficient of $S_{cancel}(t, f)$. The GD of a signal can be expressed as (20) by differentiating the phase by the angular frequency. Therefore, the GDs of $S_{leak}(t, f)$ and $S_{cancel}(t, f)$ are derived as (21) and (22) by differentiating the (18) and (19) over frequency. Moreover, GD difference between of $S_{leak}(t, f)$ and $S_{cancel}(t, f)$ is expressed as (23).

$$GD = -\frac{d\phi(\omega)}{d\omega} = -\frac{1}{2\pi} \frac{d\phi(f)}{df} \quad (20)$$

$$GD_{leak} = -\frac{1}{2\pi} \frac{d}{df} \left(-\frac{f - f_0}{f_0} \right) = \frac{1}{2\pi f_0} \quad (21)$$

$$GD_{cancel} = -\frac{1}{2\pi} \frac{d}{df} \left(-\Delta\beta \frac{f - f_0}{f_0} \right) = \frac{\Delta\beta}{2\pi f_0} \quad (22)$$

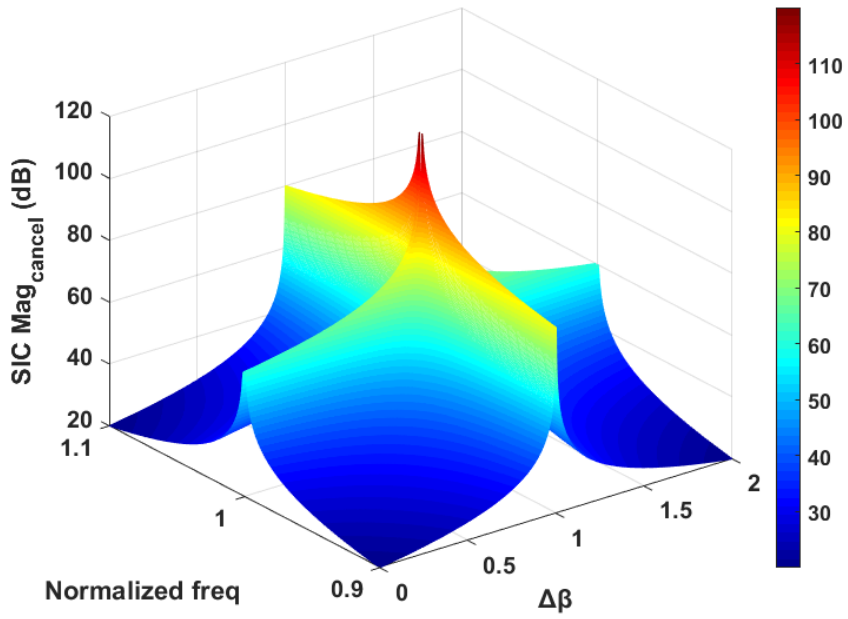
$$GD_{diff} = GD_{leak} - GD_{cancel} = \frac{1}{2\pi f_0} (1 - \Delta\beta) \quad (23)$$

It means that as $\Delta\beta$ varies from one, the GD difference of the two signals is changed. To obtain the SIC magnitude and bandwidth, (11) and (12) can develop into (24) and (25) using the above conditions.

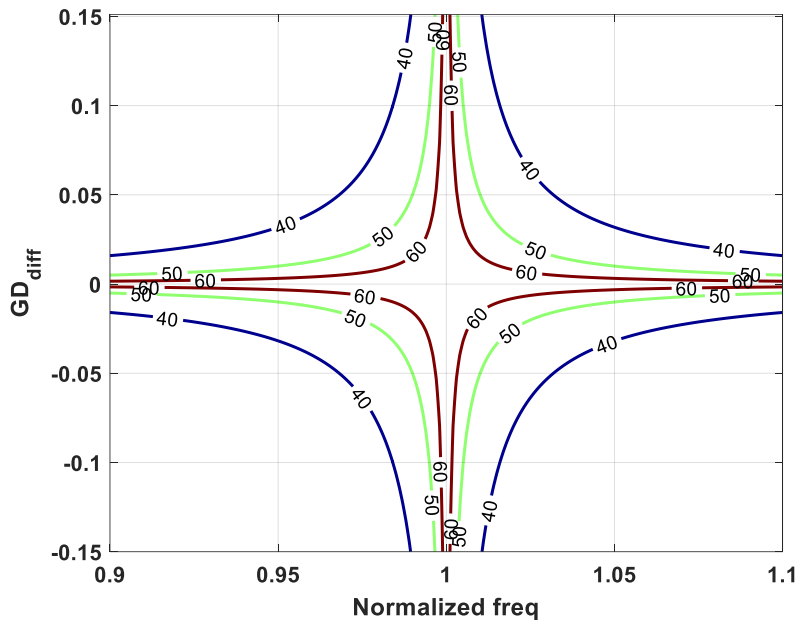
$$S_{Rx_GD}(t, f) = \cos(2\pi ft) [\cos(\theta_{leak}(f)) - \cos(\theta_{cancel}(f))] \\ - \sin(2\pi ft) [\sin(\theta_{leak}(f)) - \sin(\theta_{cancel}(f))] \quad (24)$$

$$Mag_{Rx_GD} = \sqrt{[\cos(\theta_{leak}(f)) - \cos(\theta_{cancel}(f))]^2 \\ + [\sin(\theta_{leak}(f)) - \sin(\theta_{cancel}(f))]^2} \\ = \sqrt{2 - 2\cos(\theta_{leak}(f) - \theta_{cancel}(f))} \quad (25)$$

Fig. 3.7 shows the SIC magnitude according to normalized frequencies, $\Delta\beta$ and GD_{diff} using (25). Fig. 3.7 (a) shows that the SIC magnitude is increased as $\Delta\beta$ approaches 1 and the operating frequency approaches f_0 because the phase slope constant of $\theta_{leak}(f)$ is -1. Fig. 3.7 (b) shows the SIC contours according to GD_{diff} and normalized frequencies. It shows that the 60 dB SIC magnitude bandwidth is reduced according to increment and decrement of the GD_{diff} from zero.



(a)



(b)

Fig. 3.7. SIC characteristics: (a) SIC magnitude and (b) SIC contours according to GD_{diff} and normalized frequencies

3.3 Summary and Discussion

In this chapter, the SIC magnitude and bandwidth according to the magnitude, phase and GD difference of the two signals were analyzed. In order to obtain the 60 dB SIC, very precise adjustment of the offset signal is required. However, using a circulator or a transmit/receive isolation circuit, a typical Tx/Rx isolation of 20 dB can be obtained. Additionally, 60 dB isolation is achieved by subsequent isolation of 40 dB using the SIC technique. According to the mathematical analysis, the magnitude and phase error to obtain a 40 dB SIC is 10 times wider than the 60 dB SIC. Moreover, these magnitude and phase errors should be obtained in the overall operating frequency band to realize the broadband SIC characteristic. Therefore, the IBFD RF front-end structure for similar frequency responses of the leakage signal and the cancellation signal is required for the broadband SIC.

CHAPTER 4

SINGLE ANTENNA

IN-BAND FULL-DUPELX RF FRONT-END

This section presents broadband IBFD RF front-end using circulators (CLs). Conventional IBFD RF front-end with CL can easily isolate Tx and Rx and achieve 60 dB isolation in narrowband with SIC technique. To enhance the SIC bandwidth, new structures using CLs are proposed in order to improve the 60 dB isolation bandwidth with high return loss antenna structure, and experimental results are presented.

4.1 IBFD RF Front-end using Circulator

Fig. 4.1 shows the block diagrams of the conventional and proposed IBFD RF front-end. Both structures consist of the CL, small-signal amplifier, variable phase shifter, variable attenuator, variable group delay adjuster, directional coupler, and Tx & Rx common antenna. The proposed structure replaces the Tx directional coupler with a CL compared to the conventional circuit. This

replaced CL makes the frequency characteristics of the leakage and cancellation signals similar in Rx. The basic principle of operation is that some portion of the Tx signal is passed through the leakage path to Rx because the isolation of the CL is not perfect. To reduce the leakage signal, a part of the Tx signal is transfer to Rx with the out-of-phase and the same magnitude of leakage signal through the cancellation path using Tx coupler or CL 1.

Fig. 4.2 shows the propagation characteristics of the leakage path and the cancellation paths of two IBFD RF front-ends. The leakage path can be seen that the frequency characteristics variate depending on the isolation characteristics of the CL 2. However, the cancellation path of the conventional structure shows a flat frequency response in the 200 MHz bandwidth because it implements a cancellation path using a 20 dB directional coupler. Therefore, 60 dB of isolation characteristic can only be obtained in a narrow band when SIC technique applied with these two signals.

The proposed circuit replaces the directional coupler with the CL 1. Accordingly, it shows a similar frequency characteristic between the leakage path and the cancellation path. As a result, it is suitable to obtain broadband 60 dB isolation using SIC technology because the error of the two signals according to mathematical analysis can be obtained at broadband.

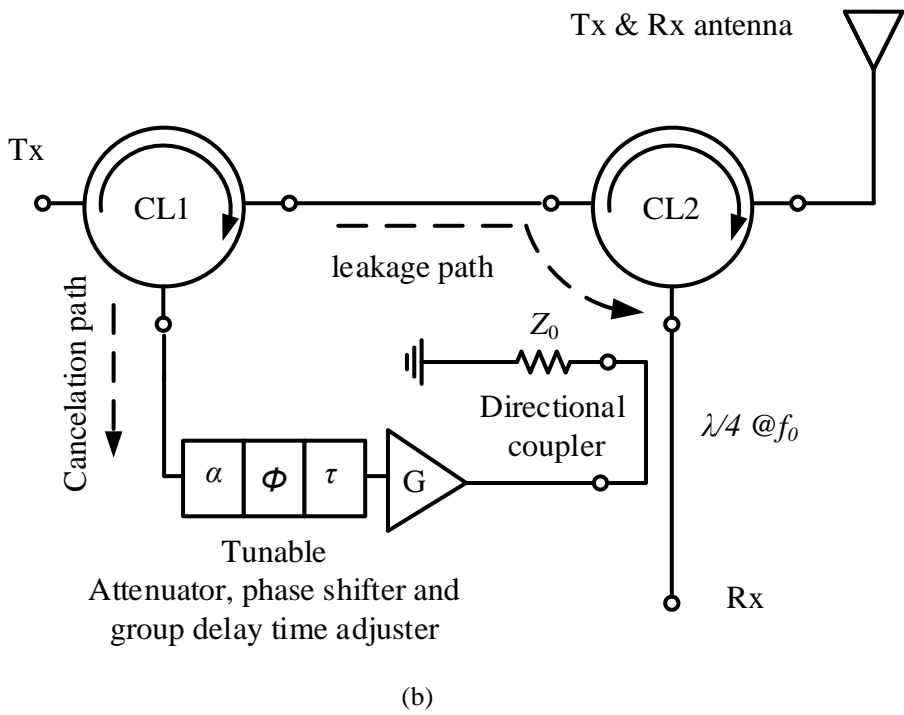
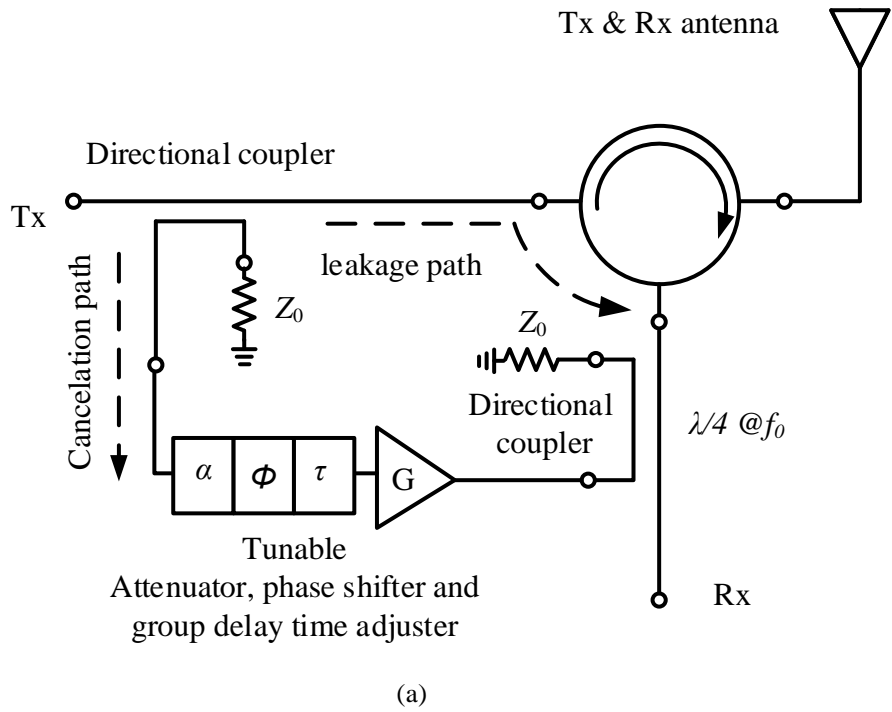


Fig. 4.1. IBFD RF front-end structures: (a) conventional and (b) proposed

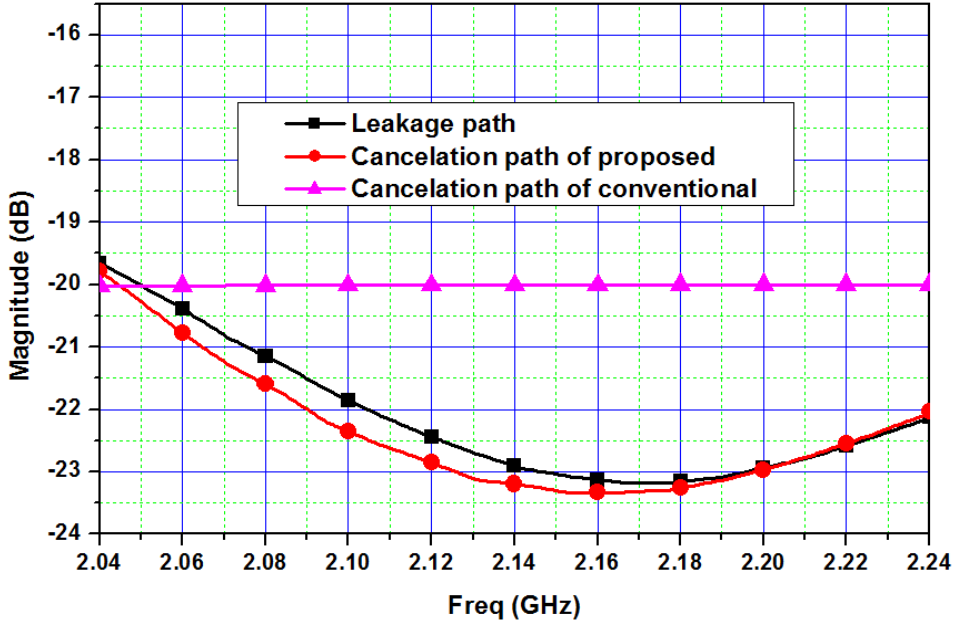


Fig. 4.2. Frequency response of leakage path and cancellation path of IBFD RF front-end structures

4.2 Analysis of Proposed IBFD RF Front-end using Circulator

Fig. 4.3 shows signal flow paths of proposed IBFD RF front-end using circulator. The each leakage and cancellation signals of the proposed structure can be analyzed as follows when the transfer characteristics of the output and isolation terminals according to the input of the circulator are represented by T_{th} $\angle \theta_{th}$ and I_{iso} $\angle \theta_{iso}$ as shown in Fig. 4.4.

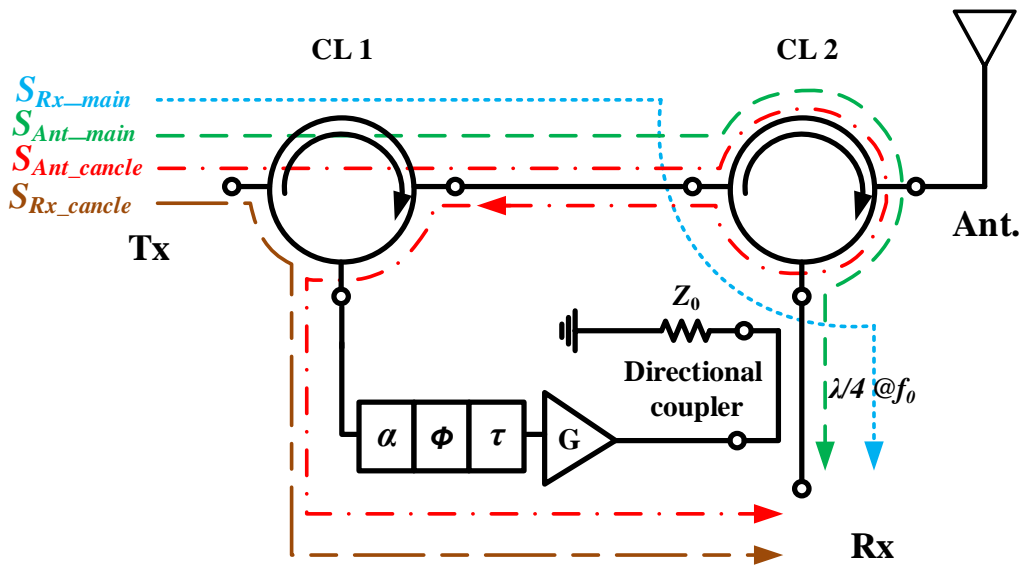


Fig. 4.3. Signal flow paths of proposed IBFD RF front-end using circulator

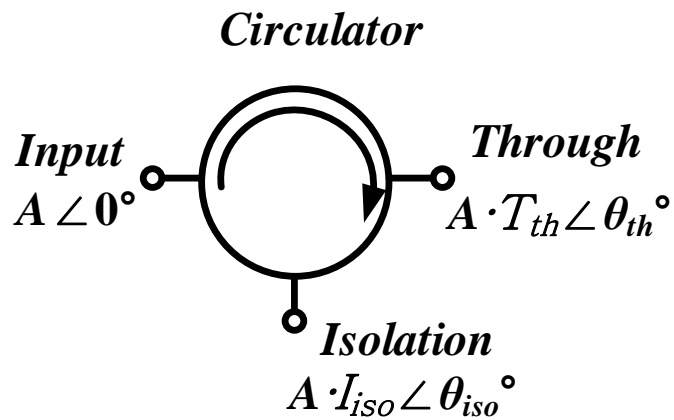


Fig.4.4. Through and isolation characteristics of circulator.

If there is no reflection of the antenna, the leakage signal S_{Rx_main} leaked from CL2 and the cancellation signal S_{Rx_cancel} generated from CL1 can be expressed as (26) and (27).

$$S_{Rx_main} = A \cdot T_{th} \cdot I_{iso} \cdot (1-c) \angle (\theta_{th} + \theta_{iso} + 0.5\pi) \quad (26)$$

$$S_{Rx_cancel} = A \cdot I_{iso} \cdot G \cdot \alpha \cdot c \angle (\theta_{iso} + \theta_{p.s.}) \quad (27)$$

where G , α , θ_{ps} , c are the gain of the small-signal amplifier, the attenuation constant of the variable attenuator, the phase constant of the variable phase shifter, and the coupling coefficient of the directional coupler, respectively. In addition, it is assumed that both the variable attenuator and the variable phase converter have no gain-phase cross-coupling characteristics, and the group delays of the main path and the cancellation path are matched.

Ideally, if there is no signal reflected from the antenna, it can be sufficiently represented by equations (26) and (27). However, the reflection characteristic of the actual antenna may be expressed as $\Gamma_{Ant} \angle \theta_{Ant}$, and these signals are also leaked into the Rx through CL1 and CL2. These S_{Ant_main} and S_{Ant_cancel} can be expressed as Equation (28) and (29).

$$S_{Ant_main} = A \cdot T_{th}^3 \cdot \Gamma_{Ant} \cdot (1-c) \angle (3\theta_{th} + \theta_{Ant} + 0.5\pi) \quad (28)$$

$$S_{Ant_cancel} = A \cdot T_{th}^3 \cdot \Gamma_{Ant} \cdot I_{iso} \cdot G \cdot \alpha \cdot c \angle (3\theta_{th} + \theta_{Ant} + \theta_{iso} + \theta_{p.s.}) \quad (29)$$

The total signal S_{total} in Rx can be express as

$$\begin{aligned}
S_{total} &= S_{Rx_main} + S_{Rx_cancel} + S_{Ant_main} + S_{Ant_cancel} \\
&= AT_{th} I_{ios} \cos(\theta_{th} + \theta_{iso} + 0.5\pi) + \frac{G\alpha A I_{ios}}{100} \cos(\theta_{iso} + \theta_{p.s.}) \\
&\quad + AT_{th}^3 \Gamma_{Ant} \cos(3\theta_{th} + \theta_{Ant} + 0.5\pi) + \frac{G\alpha AT_{th}^3 \Gamma_{Ant} I_{ios}}{100} \cos(3\theta_{th} + \theta_{Ant} + \theta_{iso} + \theta_{p.s.}) \\
&\quad + j \left(\begin{aligned}
&AT_{th} I_{ios} \sin(\theta_{th} + \theta_{iso} + 0.5\pi) + \frac{G\alpha A I_{ios}}{100} \sin(\theta_{iso} + \theta_{p.s.}) \\
&+ AT_{th}^3 \Gamma_{Ant} \sin(3\theta_{th} + \theta_{Ant} + 0.5\pi) + \frac{G\alpha AT_{th}^3 \Gamma_{Ant} I_{ios}}{100} \sin(3\theta_{th} + \theta_{Ant} + \theta_{iso} + \theta_{p.s.})
\end{aligned} \right) \quad (30)
\end{aligned}$$

For perfect isolation, the S_{total} must be a zero. Therefore, the values of α and θ_{ps} are derived from the real and imaginary part with perfect isolation condition as (31) and (32). Obtained α and θ_{ps} can be used as initial values in simulation and measurement.

$$\theta_{p.s.} = \tan^{-1} \frac{(k_2 B_1 - k_1 B_2)}{(k_2 B_2 + k_1 B_1)}, \quad (31)$$

$$\alpha = \frac{-k_1}{B_1 \cos \theta_{p.s.} - B_2 \sin \theta_{p.s.}}, \quad (32)$$

where

$$k_1 = T_{th} \cdot I_{ios} \cdot \cos(\theta_{th} + \theta_{iso} + 0.5\pi) + T_{th}^3 \cdot \Gamma_{Ant} \cdot \cos(3\theta_{th} + \theta_{Ant} + 0.5\pi) \quad (33a)$$

$$k_2 = T_{th} \cdot I_{ios} \cdot \sin(\theta_{th} + \theta_{iso} + 0.5\pi) + T_{th}^3 \cdot \Gamma_{Ant} \cdot \sin(3\theta_{th} + \theta_{Ant} + 0.5\pi) \quad (33b)$$

$$B_1 = G \cdot I_{ios} \cdot c \cdot \cos \theta_{iso} + G \cdot T_{th}^3 \cdot \Gamma_{Ant} \cdot I_{ios} \cdot c \cdot \cos(3\theta_{th} + \theta_{Ant} + \theta_{iso}) \quad (33c)$$

$$B_2 = G \cdot I_{ios} \cdot c \cdot \sin \theta_{iso} + G \cdot T_{th}^3 \cdot \Gamma_{Ant} \cdot I_{ios} \cdot c \cdot \sin(3\theta_{th} + \theta_{Ant} + \theta_{iso}) \quad (33d)$$

4.3 Experimental Results of IBFD RF Front-end using Circulator

In order to verify the proposed IBFD RF front-end using circulator, it was fabricated at the WCDMA (wideband code division multiple access) downlink band 2.14 GHz. The used circulator and PCB are ADC214CE of Admotech and Rogers Duroid 5880 teflon substrate with a thickness (h) and dielectric constant (ϵ_r) of 31 mils and 2.2, respectively. MATLAB, HFSS (high frequency structure simulator) and ADS (advanced design system) were used for simulation.

Fig.4.5 shows schematics of variable attenuator and phase shifter. To obtain high return loss, a variable attenuator and phase shifter are designed by connecting a PIN diode and a varactor diode to the coupling and transfer ports of a 3 dB hybrid coupler. The PIN diode used in the variable attenuator was HSMP-4810 of Avago and the varactor diode used in the variable phase shifter was 1T362 of Sony.

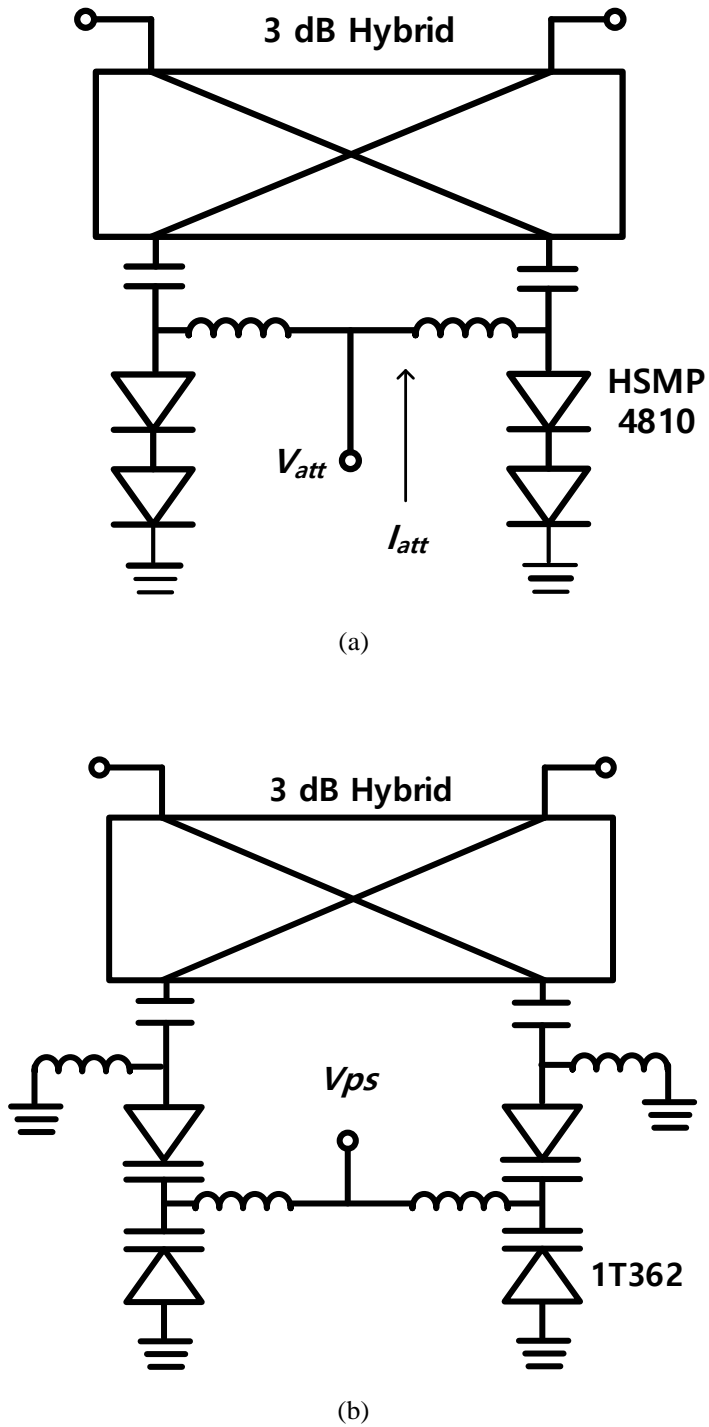


Fig. 4.5. Schematics of variable (a) attenuator and (b) phase shifter

When the internal junction resistance R_j is 50Ω according to the forward bias current of the PIN diode, reflection does not occur at the termination and it makes the largest attenuation characteristic. Fig.4.6 shows the attenuation characteristics of the designed variable attenuator at 2.14 GHz. The R_j of the PIN diode has higher resistance characteristics as the forward current is lower. Therefore, the attenuation characteristic increases as the junction resistance approach 50Ω from higher resistances while the forward current changes from 0.1 to 6.3 mA. Above 6.3 mA, the junction resistance is less than 50Ω and it causes reflections at the termination again, reducing the attenuation characteristics. Therefore, variable attenuation characteristics of -2.5 to -28.2 dB was obtained with the less than 0.34° of phase deviation.

Variable phase shifters can obtain phase variations by varying the junction capacitance of the varactor diode with a control voltage. The variable phase shifter was fabricated with two varactor diodes in each branch of hybrid to achieve a large phase-shifting range. Fig. 4.7 show phase variation characteristics of variable phase shifter with control voltage at 2.14 GHz. Phase variation range of 119.2° was obtained with the less than 0.22 dB of insertion loss deviation.

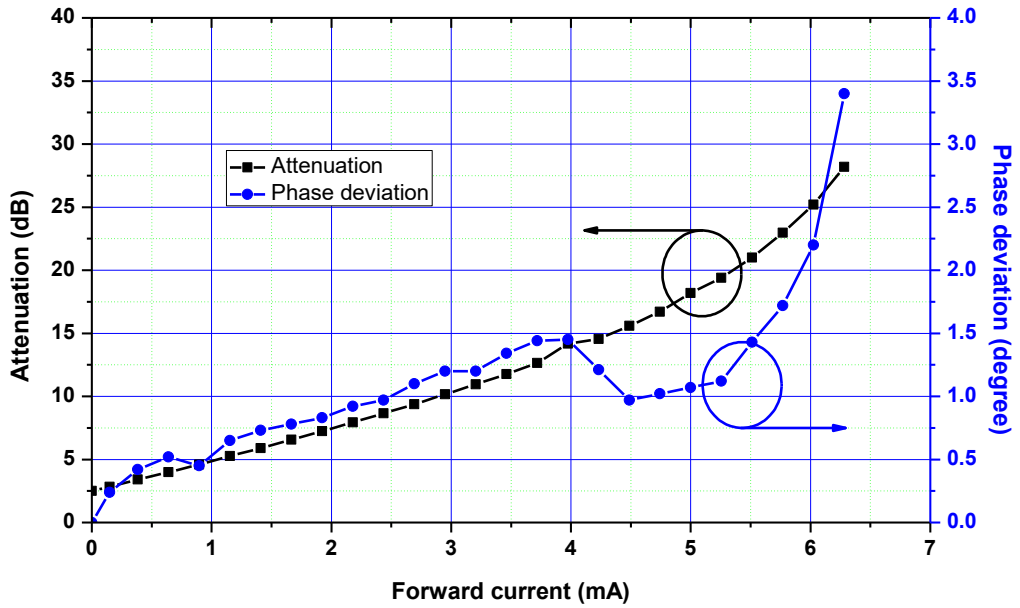


Fig. 4.6. Attenuation and phase deviation characteristics of variable attenuator according to forward current at 2.14 GHz

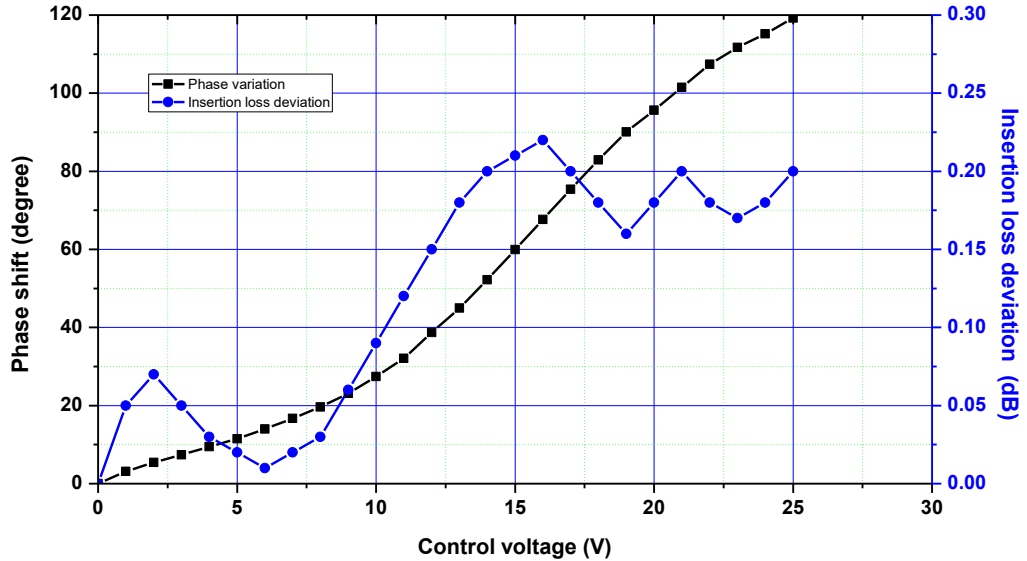


Fig. 4.7. Phase variation and insertion loss deviation characteristics of variable phase shifter according to control voltage at 2.14 GHz

In practical operation, the signal reflected from the antenna is transferred directly to Rx as a self-interference. Also, the signals S_{Ant_main} and S_{Ant_cancel} according to antenna reflection have the largest group delay difference due to the physical structure. Fig. 4.8 shows the simulated isolation characteristics according to the antenna port return loss variation. The antenna port is terminated by resistance and it has a constant return loss characteristic along with the frequency. Therefore, return loss of the antenna port is controlled by resistance. Simulation results show the isolation characteristics are degraded according to the antenna return loss decrement.

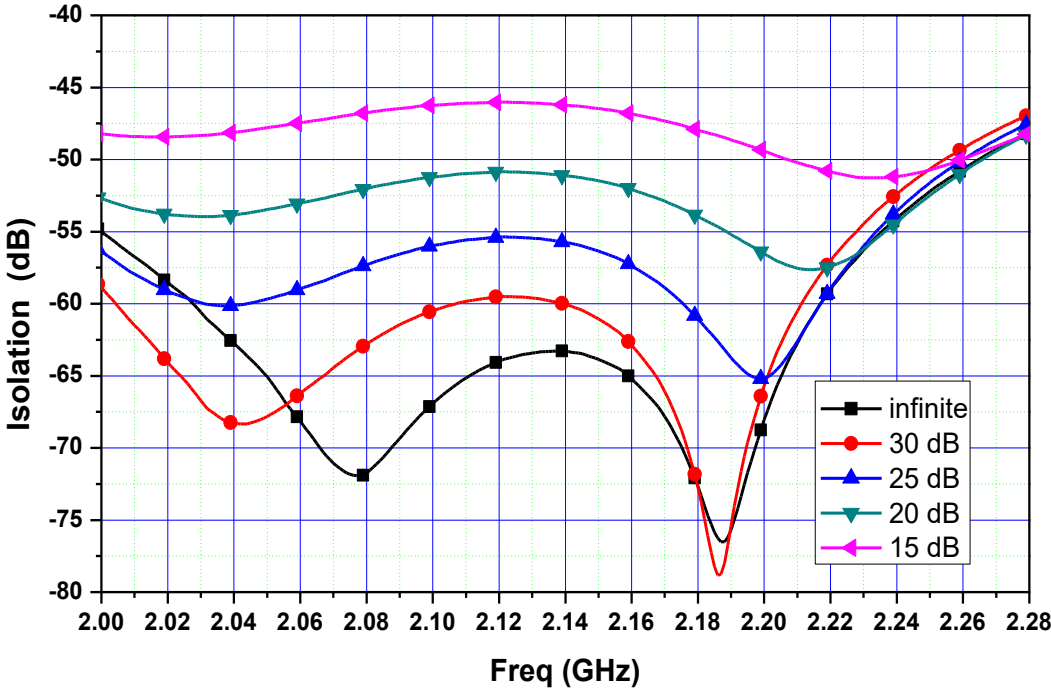


Fig. 4.8. Ideal simulation results of isolation characteristics according to return loss of antenna.

To overcome this isolation degradation, a broadband high return loss antenna of [58] was designed. Fig. 4.9 shows the geometry of broadband high return loss antenna used for the measurement. This antenna consists of a dual-polarized microstrip patch antenna with high isolation and the 90° phase offset Wilkinson power divider. Two microstrip patch antennas are fed by a 90° Wilkinson power divider. The reflected signals are combined at the Wilkinson power divider with 180° phase difference and cancel out each other when the two antennas are identical. Through this procedure, the antenna used in measurement can be obtained high reflection characteristics in the broadband. In case of reception, two signals are received at each antenna with 0° / 90° phase difference, respectively. These signals are combined in-phase by the 90° phase-offset Wilkinson power combiners and transfer to Rx.

Fig. 4.10 shows simulated broadband high return loss antenna and radiation pattern using HFSS (high frequency structure simulator). The patch of antennas and reflector are arranged horizontally in the x - y plane, and the simulation results show that the radiation pattern has directivity in the z -axis with the maximum gain of 9.2 dB.

Fig. 4.11 shows measurement results of return losses of individual patch antennas and broadband high return loss antenna with 90° phase-offset

Wilkinson power divider. The return losses of individual patch antennas (Antenna1 and Antenna2) shows a narrow peak characteristic at 2.14 GHz. 10 dB return loss bandwidth of patch antenna is 100 MHz (2.12 ~ 2.2 GHz). The overall return loss characteristic with a 90° phase-offset Wilkinson power divider shows more than 25 dB (25.4 ~ 32.2 dB) in 200 MHz bandwidth. Therefore, used broadband high return loss antenna can be reduced the SIC degradation due to the GD difference.

Fig. 4.12 shows a GD difference between S_{Rx_main} and S_{Rx_cancel} paths. The magnetic device CL has higher GD than conventional microwave circuits. Therefore, the GD matching circuit in the block diagram is replaced with RF coaxial cable because the group delay difference between the S_{Rx_main} and S_{Rx_cancel} paths is relatively small. The measured group delay difference was 0.47 ± 0.12 ns over the 200 MHz band.

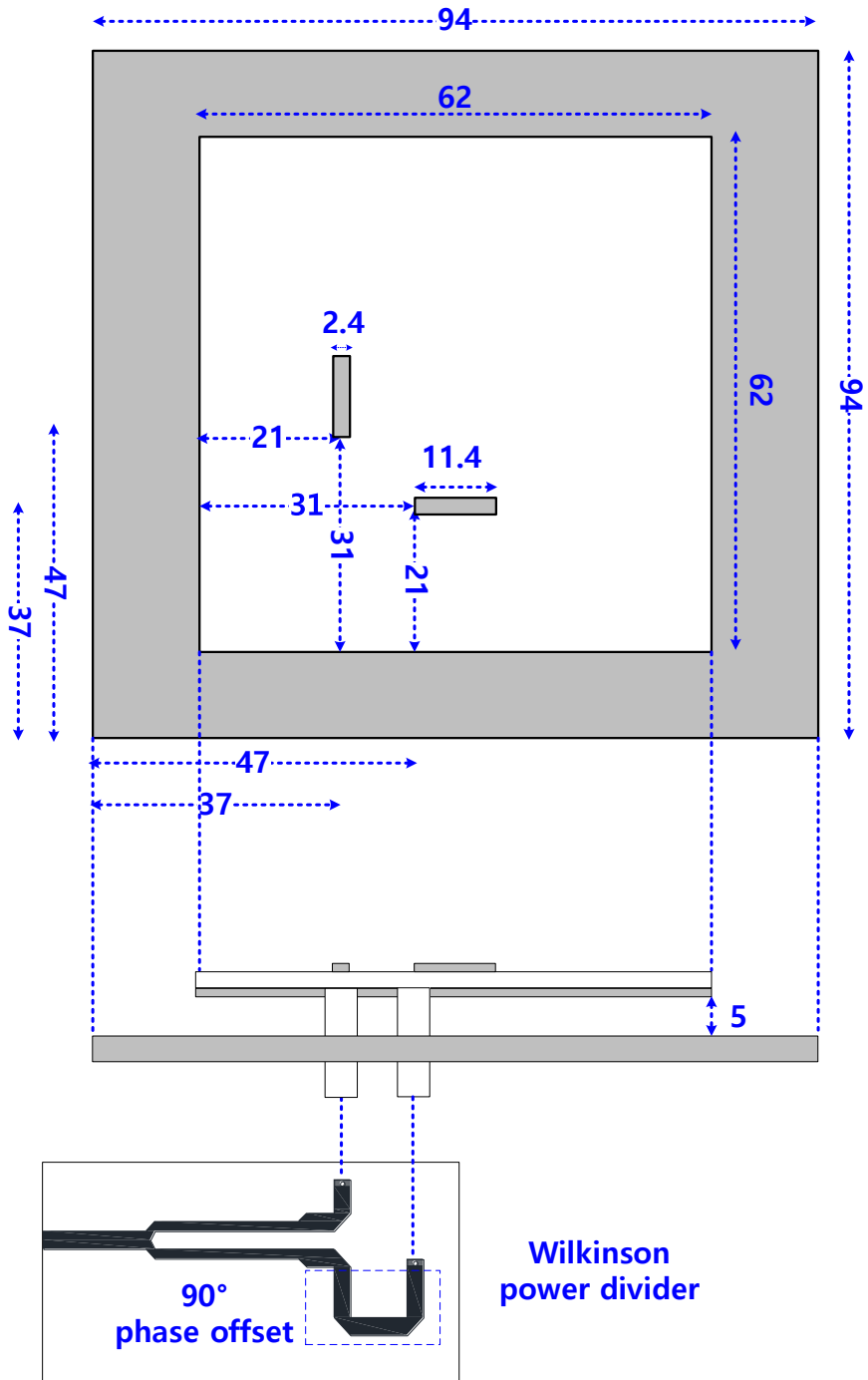
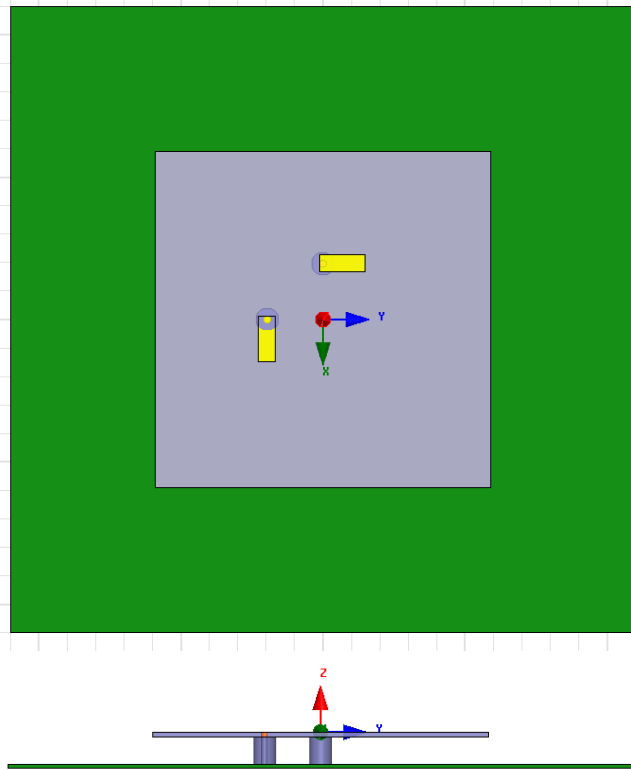
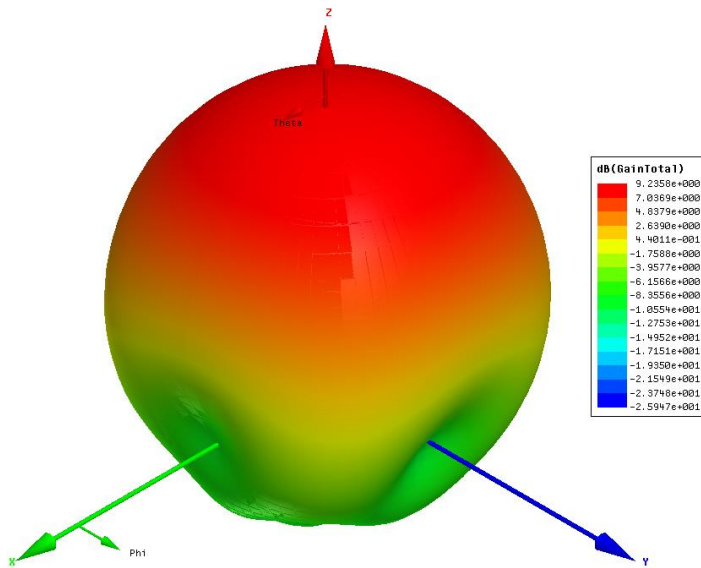


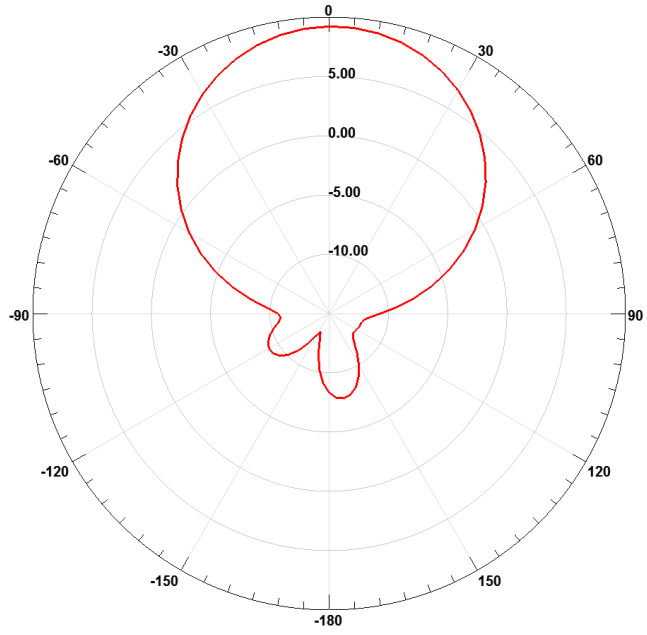
Fig. 4.9. Geometry of broadband high return loss antenna (unit: mm)



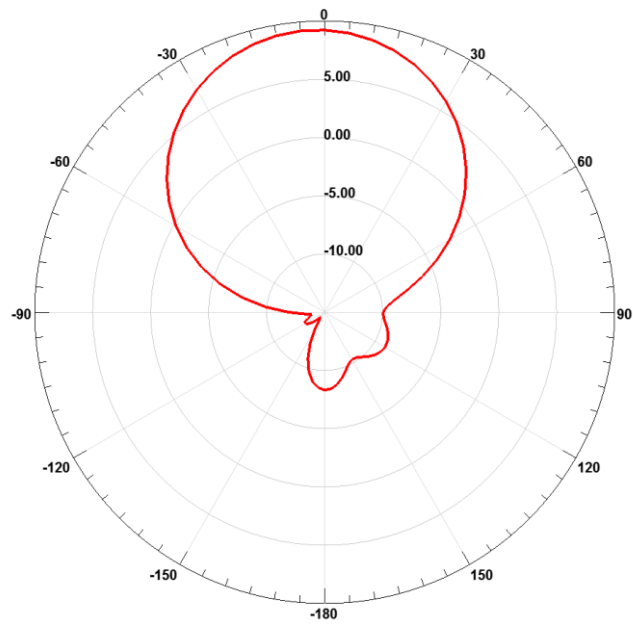
(a)



(b)



(c)



(d)

Fig. 4.10. (a) Structure of simulated in HFSS, (b) 3D radiation patter, (c) x - z plane radiation pattern (d) y - z plane radiation pattern

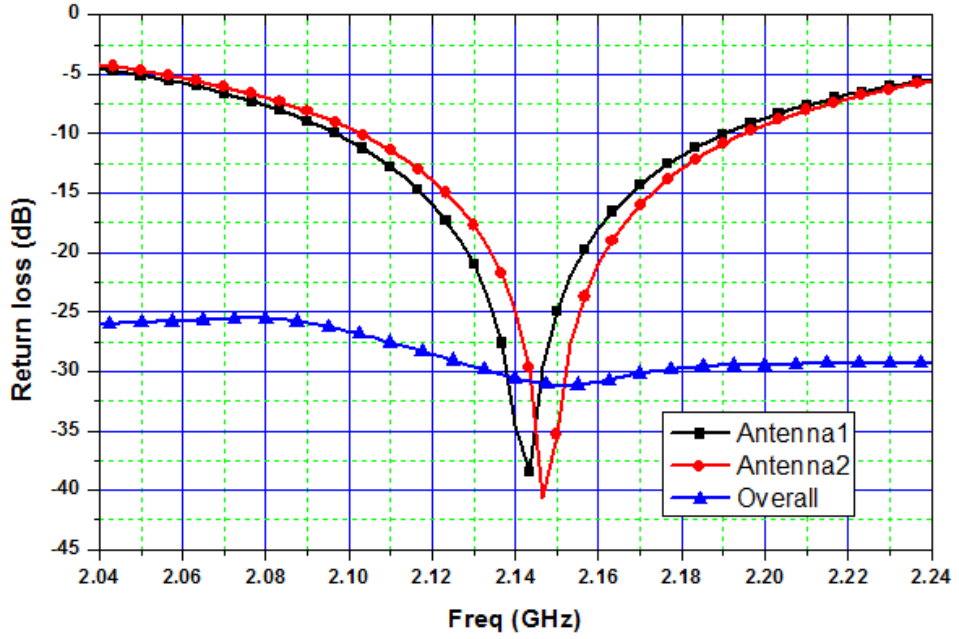


Fig. 4.11. Measured return losses of broadband high return loss antenna

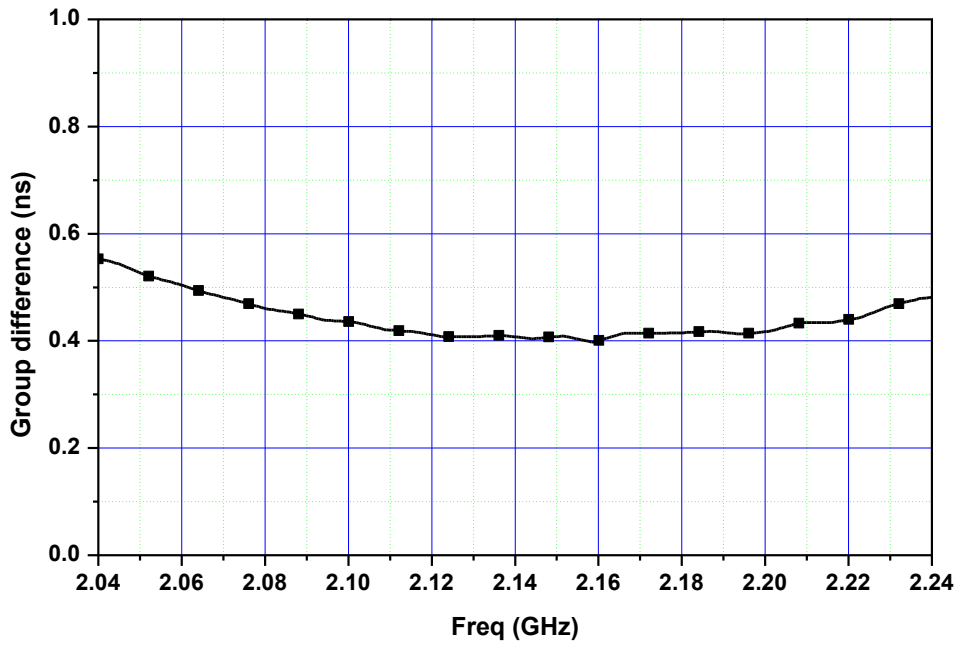


Fig. 4.12. Group delay difference between S_{Rx_main} and S_{Rx_cancel} .

The measurement results of Tx and Rx path insertion loss are shown in Fig. 4.13. The insertion loss of the Rx path is 0.55 ± 0.07 dB in the 200 MHz band because it passes through CL2 only. On the other hand, the insertion loss of Tx path is 0.83 ± 0.11 dB at the same bandwidth and it has a higher insertion loss than Rx path because the Tx signal passes through CL1 and CL2.

Fig. 4.14 and Fig 4.15 shows the photograph of measured proposed IBFD RF front-end using circulator and measurement results of Tx / Rx isolation. It can be seen that the simulation and measurement results are similar. In case of without the antenna, the simulated and measured 60 dB isolation bandwidths are 135 MHz (2.08 ~ 2.215 GHz) and 93 MHz (2.09 ~ 2.183 GHz), respectively. However, using the designed antenna, the 60 dB bandwidth is reduced to 70 MHz (2.099 ~ 2.169 GHz). This is because the isolation characteristics are degraded by the group delay difference of each path of the signal reflected from the antenna.

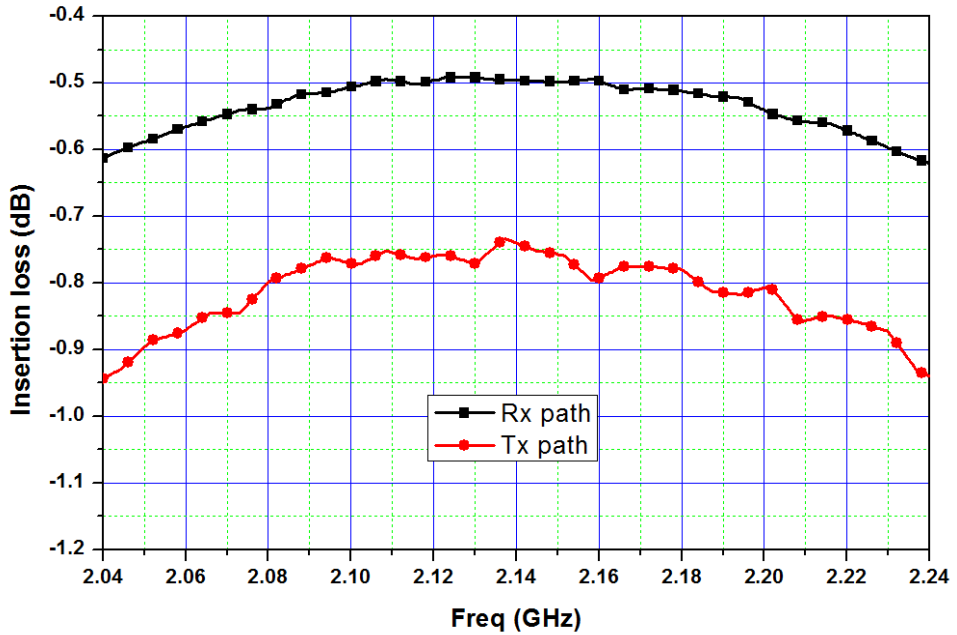


Fig. 4.13. Measured Tx and Rx path insertion losses.

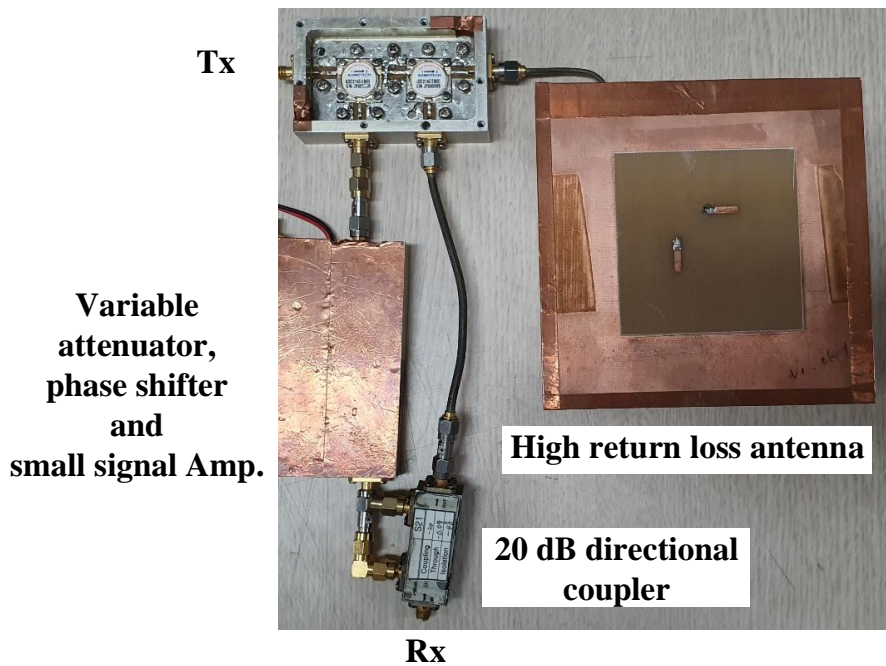


Fig. 4.14. Photograph of measured proposed IBFD RF front-end using circulator

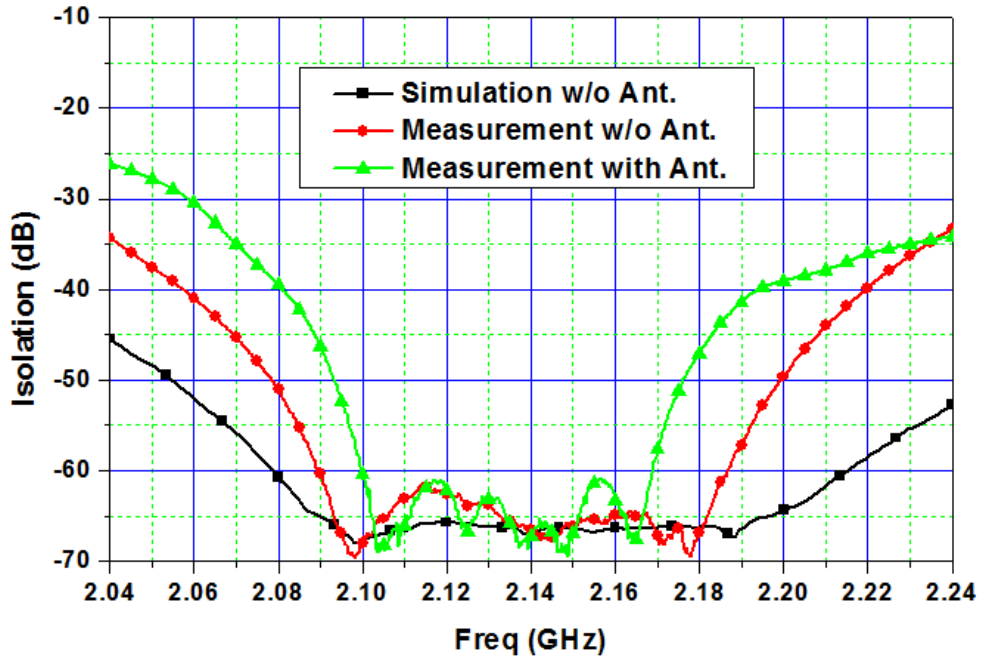


Fig. 4.15. Measured Tx / Rx isolation characteristics of proposed in-band full-duplex RF front-end using circulator

4.4 Summary and Discussion ∞

In this chapter, IBFD RF front-end using a circulator is proposed. The proposed structure realized 60 dB isolation in the 70 MHz bands using a single antenna. However, there are two issues with this structure. One is the degradation of isolation characteristic due to the antenna reflection. Another problem is isolation characteristics degraded with operating frequency increases as the usage of magnetic devices and impossible to integrate with other circuits. Therefore, in the next chapter, the in-band full-duplex RF front-end without a magnetic device is proposed.

CHAPTER 5

A MAGNETIC-FREE IN-BAND FULL-DUPLEX RF FRONT-END USING OUT-OF-PHASE BALANCING POWER SPLITTER

In this chapter, a magnetic-free IBFD RF front-end is presented. In order to overcome the drawbacks of magnetic devices such as circulator, the proposed novel IBFD RF front-end adopts broadband out-of-phase balancing power splitter (BPS) and balanced structure. The SIC characteristics according to the signals pairs in the proposed balance structure are analyzed. For validation, the experimental results of the novel magnetic-free IBFD RF front-end are provided.

5.1 Magnetic-free Balanced In-band Full-duplex RF front-end

Fig. 5.1 shows the proposed IBFD RF front-end consisting of 3-dB hybrid couplers, Wilkinson power divider/combiner, and antennas. The proposed IBFD RF front-end adopts a balanced structure (symmetric up and down) and out-of-phase balancing power splitter (BPS)^[59] for broadband SIC. All Tx

signals are transmitted through two Tx antennas after $0^\circ/180^\circ$ conversion using out-of-phase BPS. On the other hands, the signals received from two Rx antennas are combined in-phase at the Rx by Wilkinson power combiner. Therefore, it does not have any 3-dB loss, which is a basic problem of the conventional IBFD RF front-ends using a 3-dB hybrid balun and transformer.

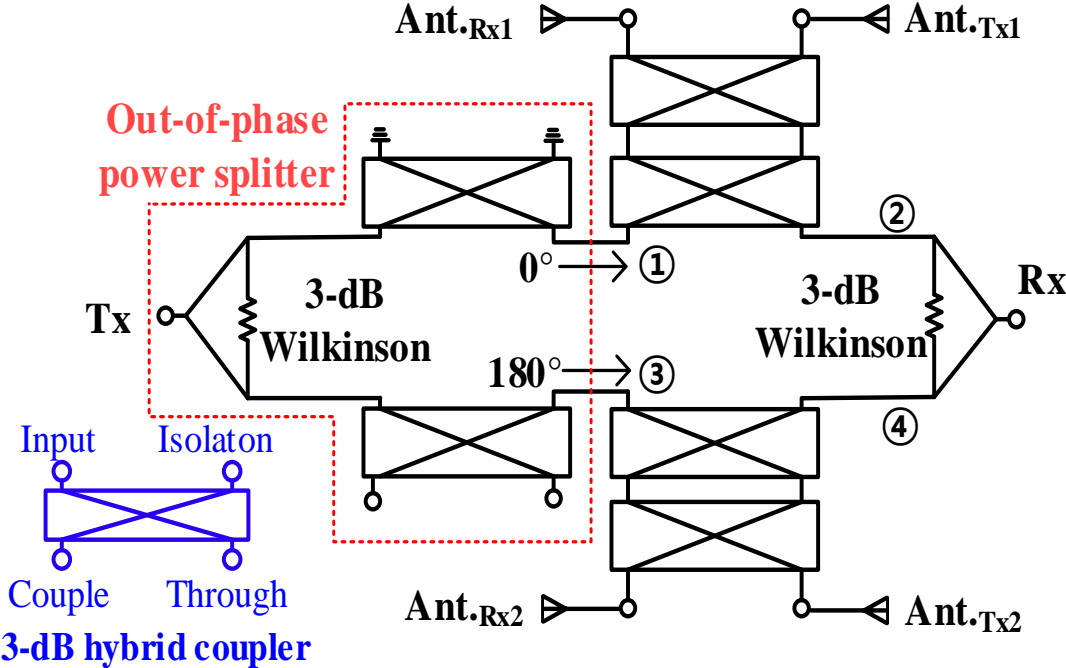


Fig. 5.1. Proposed magnetic-free in-band full-duplex RF front-end.

Fig. 5.2 shows a schematic of out-of-phase BPS and the reflective signal transmitter (RST). Out-of-phase BPS consist of a 3-dB Wilkinson power divider and two RSTs. The input signal is divided into two output signals with the same magnitude, group delay, and phase by a 3-dB Wilkinson power divider. These two divided signals pass through the RSTs with open and shorted load Z_L , respectively. (34) shows the S-parameters of RST in Fig. 5.2 (b), derived by the port reduction method^[60]. The transmission coefficient (S_{21}) of RST is controlled by the reflection coefficient Γ_L .

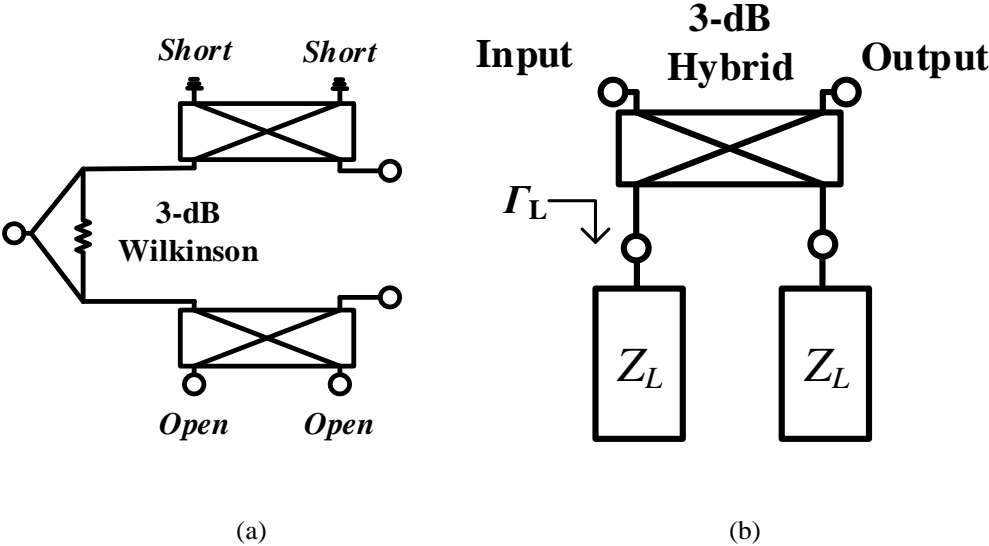


Fig. 5.2. (a) Out-of-phase balancing power splitter and (b) reflective signal transmitter.

$$S_{RST} = \begin{bmatrix} 0 & -j\Gamma_L \\ -j\Gamma_L & 0 \end{bmatrix} \quad (34)$$

(35) shows the Γ_L according to termination impedance Z_L . According to the open and short conditions, the Γ_L can have the same magnitude and opposite sign. Therefore, the proposed out-of-phase BPS has a 180° phase difference between the two output signals with the same magnitude and group delay.

$$\Gamma_{L_short} = \left. \frac{Z_L - Z_0}{Z_L + Z_0} \right|_{Z_L=0} = -1 \quad (35a)$$

$$\Gamma_{L_open} = \left. \frac{Z_L - Z_0}{Z_L + Z_0} \right|_{Z_L=\infty} = 1 \quad (35b)$$

Due to the balanced structure of the proposed IBFD RF front-end, there are pairs of Tx leakage signals into the Rx. Fig. 5.3 shows the paths of Tx leakage signal pairs in the proposed structure. The first leakage pair signals are $S_{leak_H_up}(t, f)$ and $S_{leak_H_down}(t, f)$, which pass through the 3-dB hybrid couplers due to the non-ideal isolation characteristic of the hybrid. The second and third leakage pair signals are $S_{leak_T1R1}(t, f)$, $S_{leak_T2R2}(t, f)$ and $S_{leak_T1R2}(t, f)$, $S_{leak_T2R1}(t, f)$, respectively, which are caused by cross-coupling among the Tx and Rx antennas. Table I shows the leakage signal names and their detailed paths. Each

leakage pair signal with the same magnitude and phase variations depending on time and frequency can cancel each other out at the Rx due to the dividing characteristic of out-of-phase BPS. Therefore, the mathematical model in chapter 3.1 can be used to analyze the SIC characteristics of the proposed structure according to the characteristics of these leakage signal pairs.

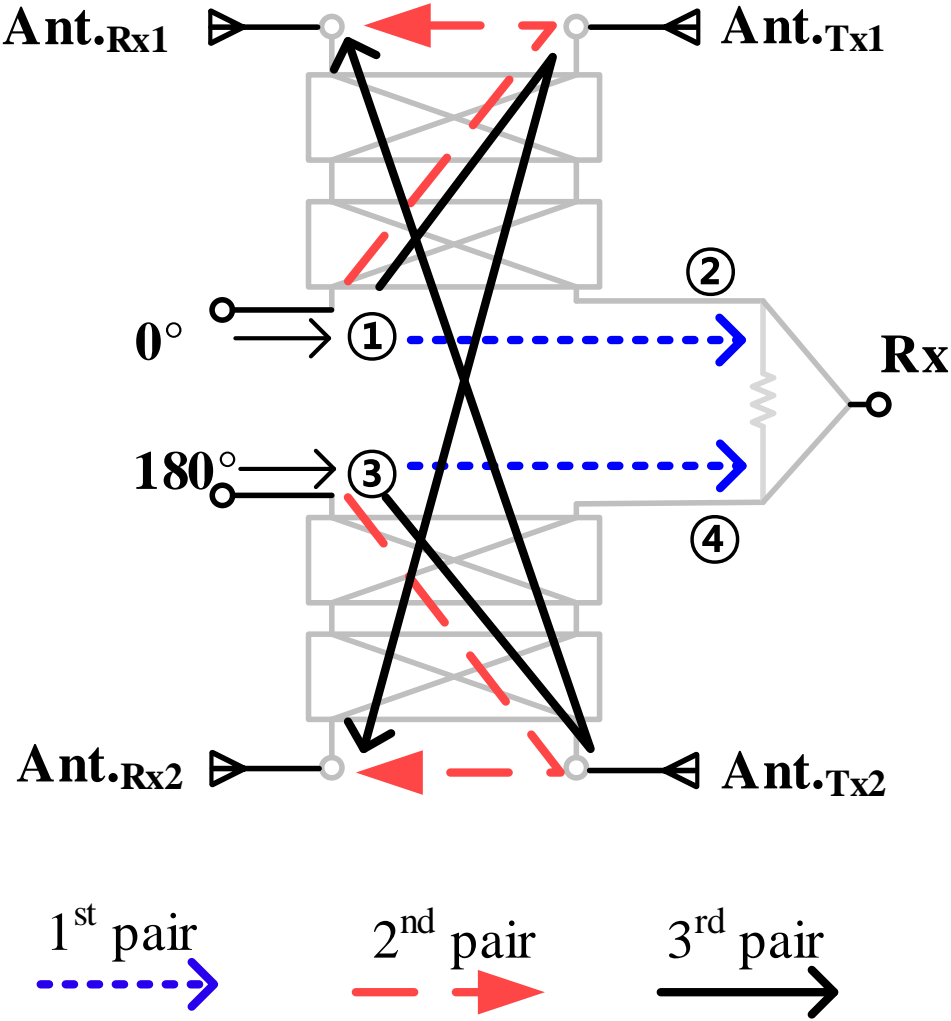


Fig. 5.3. Paths of leakage Tx signal pairs in proposed magnetic-free IBFD RF front-end.

TABLE II
LEAKAGE PAIRS AND PATHS IN PROPOSED IBFD RF FRONT-END

	Names	Paths
1st Pair	$S_{leak_H_up}(t, f)$	①-②
	$S_{leak_H_down}(t, f)$	③-④
2nd Pair	$S_{leak_T1R1}(t, f)$	①-Ant. T_{x1} -Ant. R_{x1} -②
	$S_{leak_T2R2}(t, f)$	③-Ant. T_{x2} -Ant. R_{x2} -④
3rd Pair	$S_{leak_T1R2}(t, f)$	①-Ant. T_{x1} -Ant. R_{x2} -④
	$S_{leak_T2R1}(t, f)$	③-Ant. T_{x2} -Ant. R_{x1} -②

5.2 Evaluation of Out-of-phase Balancing Power Splitter

In the chapter 3.1, the SIC characteristics were analyzed with various kinds of signal conditions such as case 1 and case 2. However, these assumptions are not the practical frequency responses in real measurement. Still, these analyses can provide a design strategy of the proposed IBFD RF front-end. Therefore, the comparison results of SIC simulation and measurement using the actual magnitude and phase responses of 0°/180° power splitters are presented in this section.

The proposed magnetic-free IBFD RF front-end adopts out-of-phase BPS for high SIC between the Tx and Rx. Fig. 5.4 shows the schematics of ring hybrid and microstrip wideband balun structures^[61] are generally used for 0°/180° power splitting. However, ring hybrid and balun structures cannot have broadband high SIC characteristics due to the narrow band out-of-phase and different GD characteristics which are caused by the different physical lengths in two power splitting paths. Therefore, the out-of-phase BPS structure is proposed to realize the equal magnitude, same GD, and out-of-phase transmission characteristics between two power splitting paths over a wide frequency bandwidth.

In order to verify the 0°/180° equal power division, the signal cancellation characteristics were simulated and measured by combining two output signals of 0°/180° power splitters with the Wilkinson power combiner, as shown in Fig. 5.5. In the Matlab simulation, (8) as well as the measured magnitudes and phases of the two paths were used for the $a_{leak}(f)$, $a_{cancel}(f)$, $\theta_{leak}(f)$, and $\theta_{cancel}(f)$. These measured data were included in all the magnitude and phase information. Therefore, A_{leak} and A_{cancel} are set to 1.

Fig. 5.6 shows a comparison of the signal cancellation characteristics among the proposed out-of-phase BPS, ring hybrid, and microstrip wideband balun at

2.5 GHz. The proposed out-of-phase BPS shows the widest and highest SIC characteristics among all of the circuits. The ring hybrid shows high cancellation characteristics only in the narrowband because it has the $0^\circ/180^\circ$ phase splitting characteristic at the center frequency. Microstrip wideband balun shows a relatively wider cancellation bandwidth than ring hybrid, but its cancellation is inferior to the proposed out-of-phase BPS. Therefore, the proposed out-of-phase BPS suitable for implementation of the broadband SIC circuit.

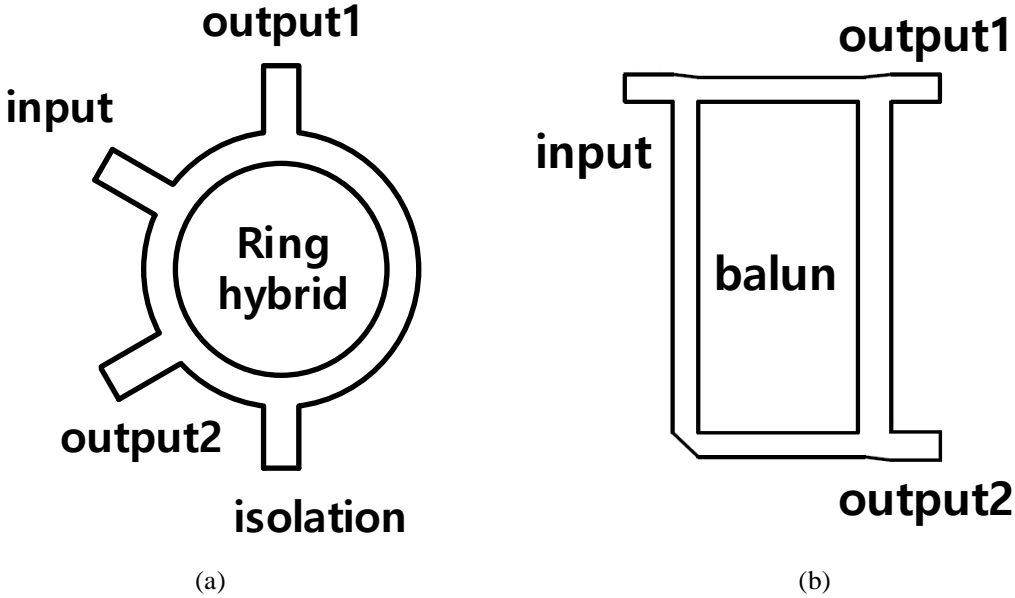


Fig. 5.4. Schematics of (a) ring hybrid and (b) microstrip wideband balun

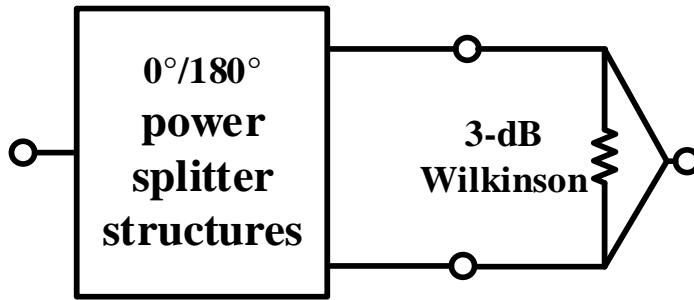


Fig. 5.5. Signal cancellation measurement set up of 0°/180° power splitter.

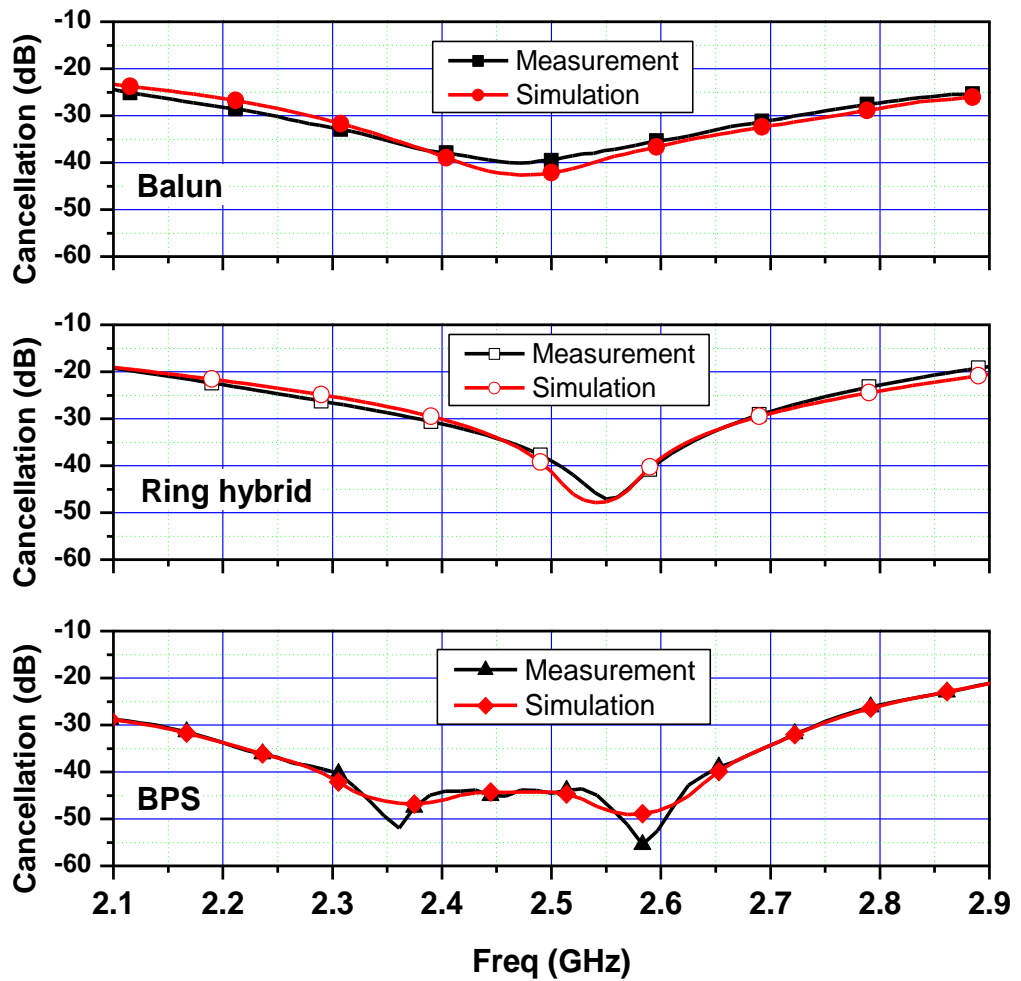


Fig. 5.6. Comparison of simulation and measurement results of 0°/180° power splitter structures.

5.3 Experimental Results of Balanced IBFD RF Front-end

In order to verify the proposed magnetic-free IBFD RF front-end, the proposed structure was implemented at 2.5 GHz WiMax frequency band. The proposed structure was fabricated on an RT/Duriod 5880 substrate PCB obtained from Rogers, Inc. with a dielectric constant (ϵ_r) of 2.2 and thickness (h) of 31 mils. The used hybrid couplers and dipole antennas are S03A2500N1 of Anaren and MAF94028 of Laird, respectively.

Fig. 5.7 shows a photograph of the fabricated magnetic-free IBFD RF front-end using out-of-phase BPS. The circuit size is $10 \times 9 \text{ cm}^2$. Fig. 5.8 shows the insertion loss of two Tx paths and the return losses at the Tx / Rx ports. As a measurement result, the insertion losses of both Tx paths in the 200 MHz bandwidth are $3.337 \pm 0.058 \text{ dB}$. Considering the transmitted power of both paths, the total insertion loss of the output is 0.34 dB at f_0 . It shows that the proposed IBFD RF front-end removes the 3 dB insertion loss of the previous circuits. Return losses at Tx and Rx ports are measured more than 18.7 dB in all 200 MHz bandwidth. Fig. 5.9 shows the noise figure measured on the Rx path. In the 200 MHz bandwidth, the noise figure is $0.587 \pm 0.1 \text{ dB}$.

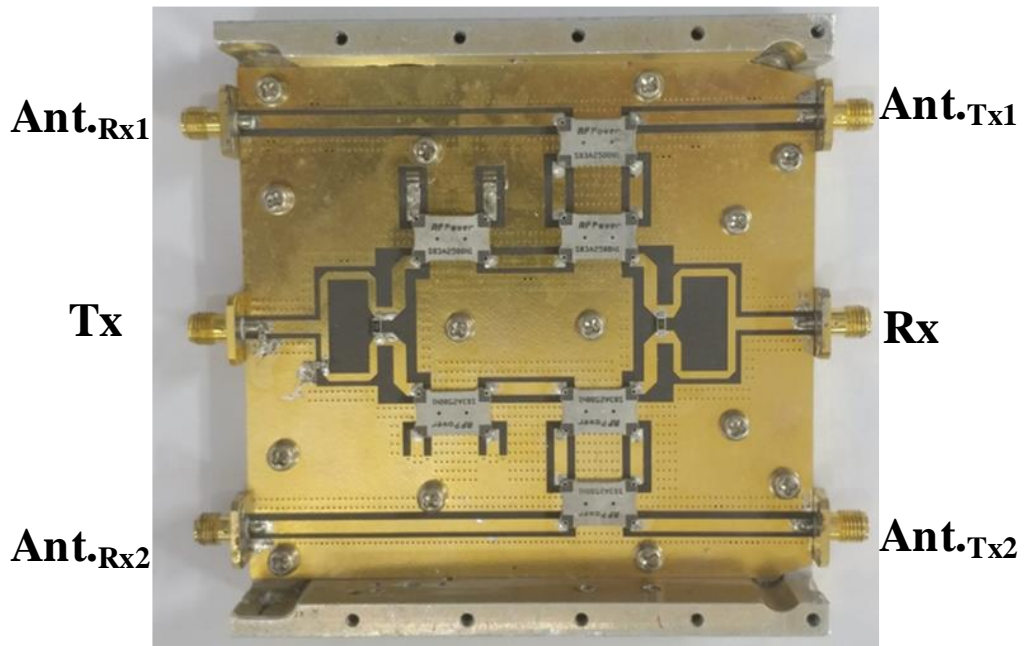
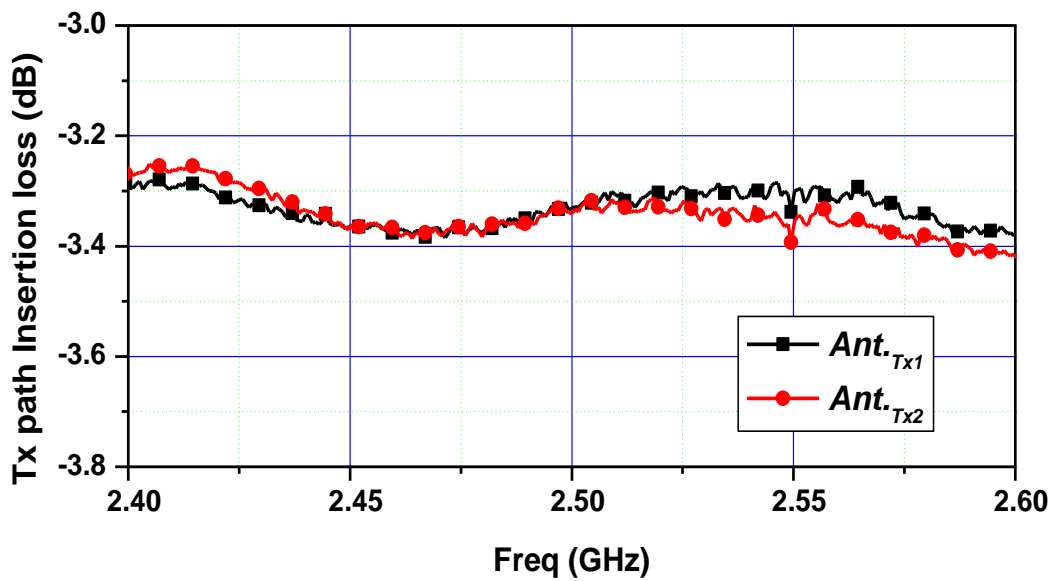
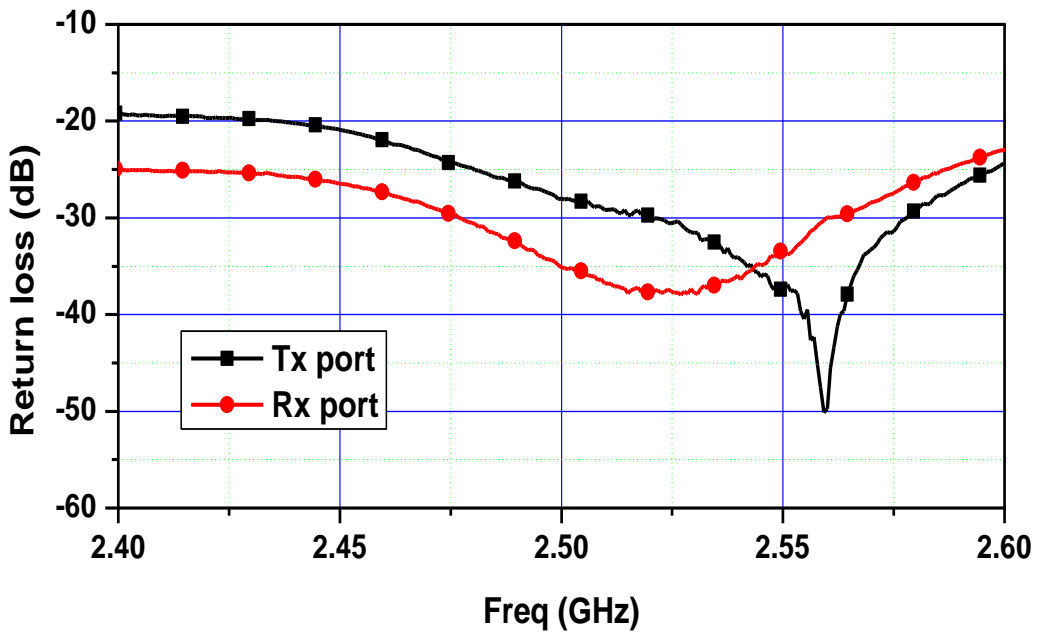


Fig. 5.7. Photograph of the fabricated magnetic-free in-band full-duplex circuit.



(a)



(b)

Fig. 5.8. Measured (a) insertion losses at two Tx paths and (b) return losses at Tx and Rx ports.

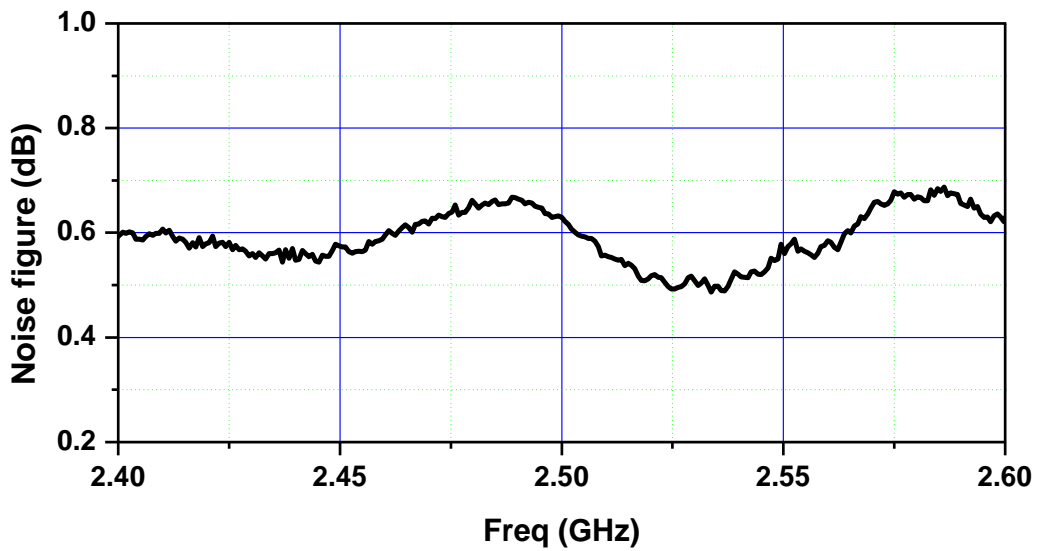


Fig. 5.9. Measurement results of noise figure at Rx.

Fig. 5.10 shows the antenna setup block diagram used for SIC measurements. The proposed IBFDC uses two antennas each in Tx and Rx paths, respectively. Accordingly, the SIC characteristics can be changed due to the position and distance of the antennas. Tx and Rx Antennas are arranged on the $\pm y$ -axis and the $\pm x$ -axis with distance d from the center, respectively.

Fig. 5.11 shows the simulated radiation patterns of the dipole antennas using the HFSS. The maximum gains are 6.2 dB, 5.1 dB, and 4.1 dB when d is 15 mm, 30 mm, and 45 mm, respectively. Among the d variations, the maximum gain is obtained at $d = 15$ mm which is a quarter of wavelength distance ($2d = \lambda/4 = 30$ mm) between antennas at 2.5 GHz.

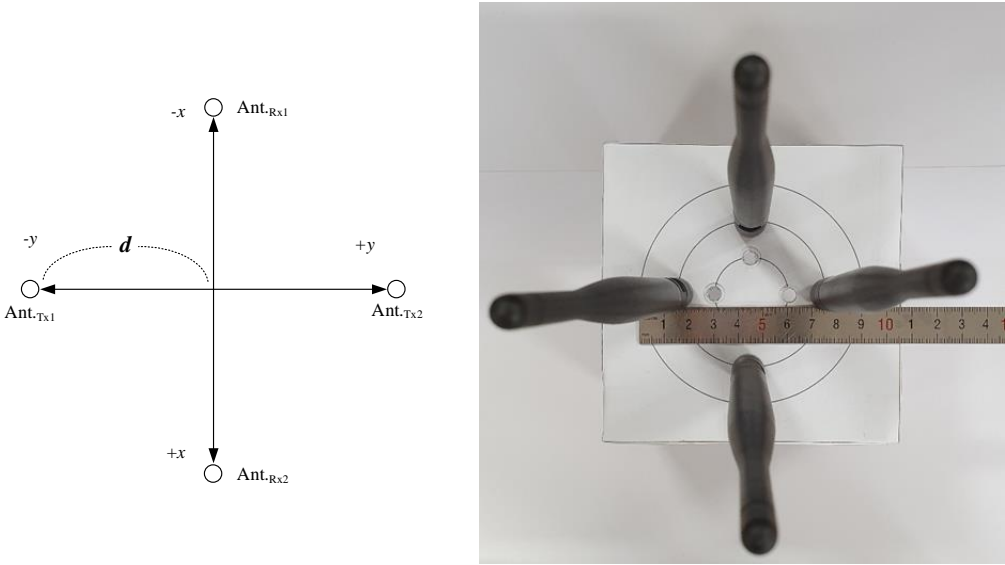
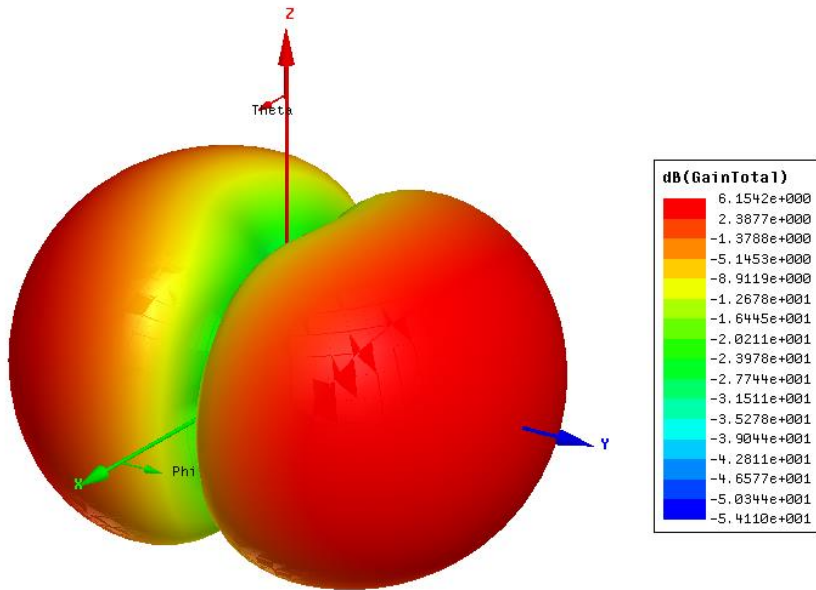
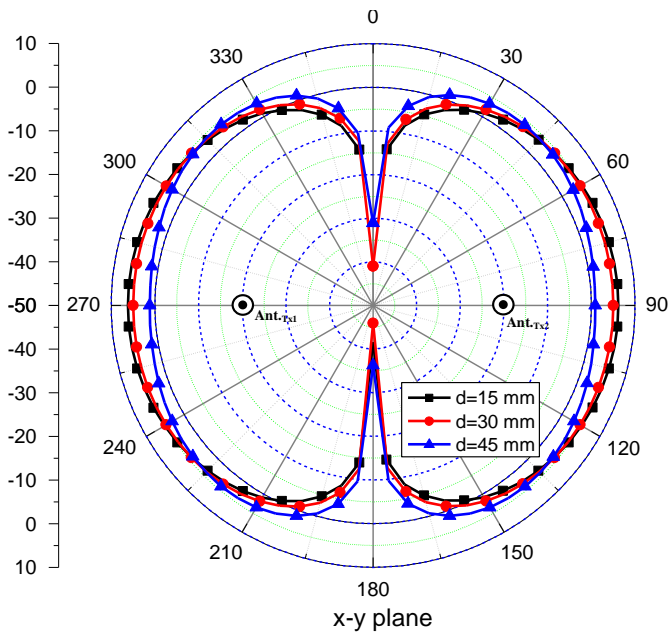


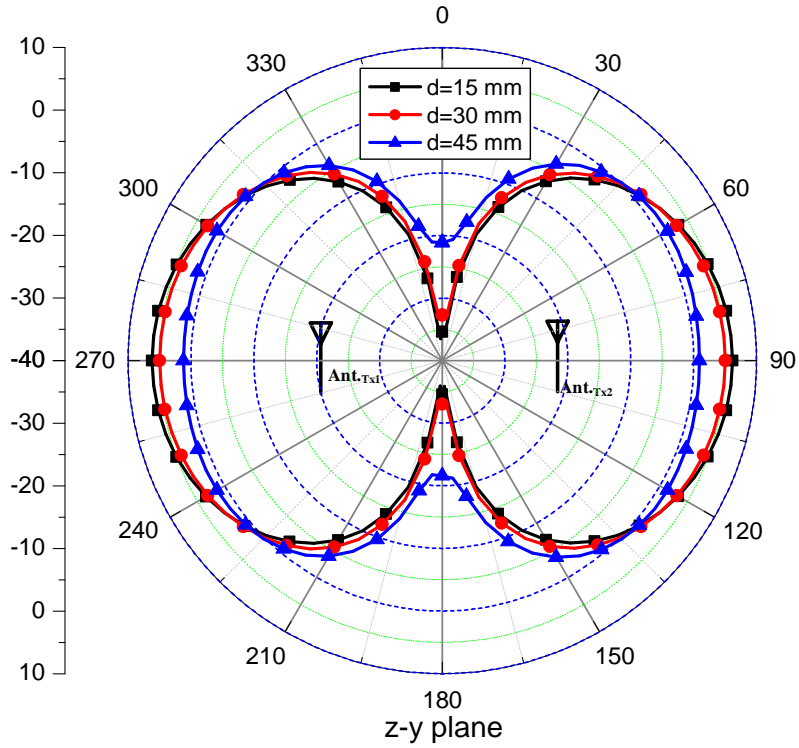
Fig. 5.10. Block diagram and photograph of antennas setup for SIC measurement.



(a)



(b)



(c)

Fig. 5.11. Simulated radiation patterns with to d : (a) 3D, (b) x - y plane and (b) z - y plane at 2.5 GHz.

Fig. 5.12 shows the measured Tx-to-Rx isolation characteristics of the proposed magnetic-free IBFD RF front-end according to d . When the antenna ports are terminated at 50Ω (without antennas), the 60 dB isolation bandwidths is 190 MHz (2.37~2.56 GHz). In the case of without antennas, there is no cross-coupling among the antennas, so only the first leakage pair signals are canceled out at the Rx port. Therefore, the SIC characteristic without antennas is better than SIC with antennas.

The 60 dB isolation bandwidths with four commercial dipole antennas are measured 80 MHz (2.464 ~ 2.544 GHz) and 113 MHz (2.446 ~ 2.559 GHz) when d is 30 mm and 45 mm, respectively. When d is 15 mm, the amount of the coupling between the Tx and Rx antennas is large and 60 dB SIC characteristics cannot be obtained. The 50 dB SIC bandwidth and maximum SIC with $d = 15$ mm are 70 MHz (2.46 ~ 2.53 GHz) and 59.5 dB, respectively.

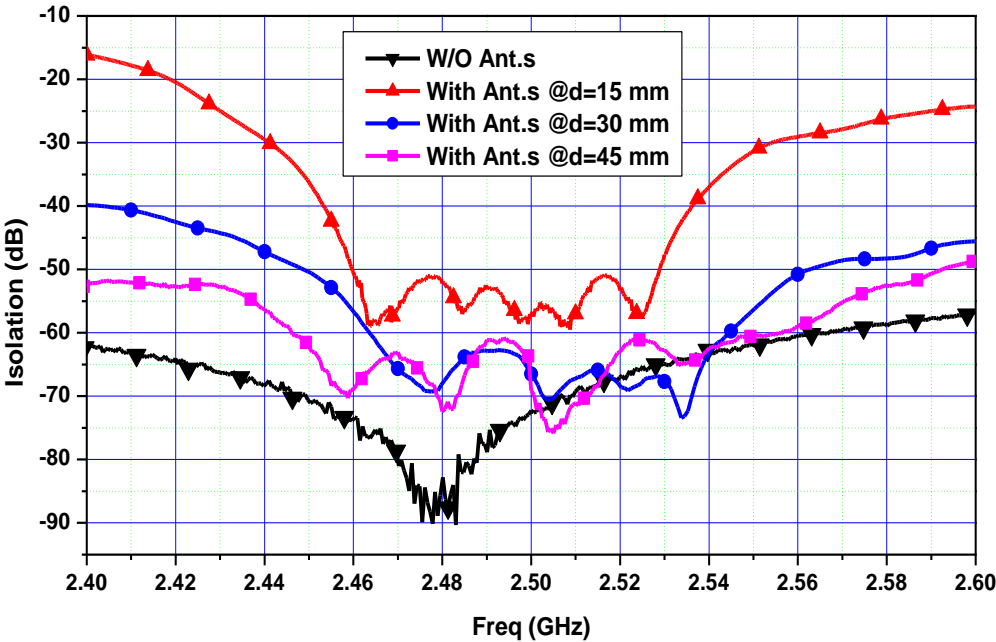


Fig. 5.12. Measured isolation characteristics of proposed magnetic-free in-band full-duplex RF front-end according to d .

Table II shows a comparison of the electrical performances among the state-of-art IBFDCs. The proposed IBFD RF front-ends has the widest SIC bandwidth and the best SIC characteristic among the works using antennas and RF front-end SIC circuits.

TABLE III
ELECTRICAL PERFORMANCES COMPARISON WITH STATE-OF-ART
IN-BAND FULL-DUPLEX RF FRONT-ENDS

Ref.	f_0 [GHz]	SIC BW [MHz]	FBW [%]	Magnetic device	Structure
[51]	2.4	50 @ 60 dB	2.08	Magnetic-free	Antenna SIC RF front-end
[52]	4.6	300 @ 50 dB	6.52	Magnetic-free	Antenna SIC RF front-end
[54]	0.914	26 @ 45 dB	2.84	Circulator	RF front-end SIC circuit
[55]	2.4	10 @ 45 dB	0.4	Magnetic-free	RF front-end SIC circuit
[57]	1.95	100 @ 52 dB	5.13	Circulator	Balance RF front-end SIC circuit
Ch. 4	<u>2.14</u>	<u>70 @ 60 dB</u>	<u>3.2</u>	<u>Circulator</u>	<u>RF front-end</u> <u>SIC circuit</u>
Ch. 5	<u>2.5</u>	<u>210 @ 50 dB,</u> <u>$d = 45$ mm</u> <u>113 @ 60 dB,</u> <u>$d = 45$ mm</u>	<u>8.4</u> <u>4.52</u>	<u>Magnetic-free</u>	<u>Balanced</u> <u>RF front-end</u> <u>SIC circuit</u>

5.4 Summary and Discussion

In this chapter, a magnetic-free in-band full-duplex RF front-end is presented. In order to realize the broadband self-interference cancellation (SIC) characteristics, the broadband out-of-phase balancing power splitter (BPS) and balanced structure are proposed and verified. In the proposed structure, the SIC characteristics of the leakage signal pairs due to the balanced structure and cross-couplings among the antennas are described.

The fabricated IBFD RF front-end characteristics are measured using commercial dipole antennas. The simulation and measurement results are consistent with each other. In the measurement results, the proposed magnetic-free IBFD RF front-end has 60 dB isolation characteristics or more over the wide frequency band. Moreover, the proposed magnetic-free IBFD is possible to implement and integrate in RF and microwave frequency bands.

CHAPTER 6

CONCLUSION AND FUTURE WORK

This chapter presents the conclusion of this dissertation and some future research directions of RF front-end for in-band full-duplex systems.

6.1 Conclusion

This dissertation presents the mathematical analysis of the signal condition to obtain 60 dB isolation and the implementation of a new in-band full-duplex (IBFD) RF front-end with broadband 60 dB isolation. The SIC technique was used to realize the broadband 60 dB Tx and Rx isolation. Therefore, analysis of the signal cancellation characteristics according to the various conditions between the leakage signal and cancellation signal was presented. Moreover, new IBFD RF front-end structures to obtain the broadband 60 dB isolation are proposed.

Chapter 2 shows the basic operation of the IBFD system and requirements. The concept of the IBFD system is briefly explained and compared to the

conventional TDD and FDD systems. Also, the specific requirements for the IBDC system were presented. In a short word, the main purpose of the RF stage in the IBFD system is realized pass band SIC technique. Therefore, this dissertation focused on the IBFD front-end structures to realize the broadband SIC characteristic.

Chapter 3 shows the mathematical analysis for the SIC technique. It presents the SIC characteristics and bandwidth according to the magnitude, phase and GD difference of the two signals with time and frequency variant signal. To obtain the 60 dB SIC, very precise adjustment of the offset signal is required. However, using a circulator or a Tx / Rx isolation circuit typical isolation of 20 dB can be obtained. Therefore, 60 dB isolation can be achieved by subsequent isolation of 40 dB using the SIC technique.

In Chapter 4, IBFD RF front-end using a circulator was proposed. Two circulators used for the broadband SIC technique for Tx and Rx 60 dB isolation. This structure achieved 60 dB isolation in the 79 MHz frequency bands using a high return loss single antenna. However, as the operating frequency increases, the isolation characteristics degrade and it is impossible to integrate with other circuits as the usage of the magnetic device. Therefore, in the next chapter, the in-band full-duplex RF front-end without a magnetic device was proposed.

Chapter 5 proposed a magnetic-free IBFD RF front-end using out-of-phase balancing power splitter. To eliminate the disadvantages of the magnetic devices, a novel magnetic-free IBFD RF front-end presented. To realize the broadband SIC characteristics, the broadband out-of-phase balancing power splitter (BPS) and the balanced structure was proposed and verified. The fabricated magnetic-free IBFD RF front-end characteristics are measured using commercial dipole antennas. The proposed magnetic-free IBFD RF front-end achieved 113 MHz 60 dB isolation bandwidth with antennas. Moreover, the proposed magnetic-free IBFD is possible to implement and integrate at microwave frequency bands and over.

6.2 Future work

This dissertation is focused on the structures for implementing wideband transmit/receive isolation characteristics in the RF front-end. Of course, a lot of research on the analog and digital stages are in progress, but various studies are also underway in the RF field.

One topic is the study of combining the MIMO and IBFD systems. Many studies have already been conducted to improve data transmission efficiency by combining MIMO and IBFD. However, in a MIMO system having multiple transmit and receive paths, the coupling among each transmitter and receiver

occurs and thus a complex leakage signal and a path occurred. Therefore, these complex leakage signals should be removed to realize the IBFD with MIMO. It is difficult to obtain broadband characteristics even in a single transmit/receive state. Therefore, studies on various mathematical models and cancellation techniques are required to realize the IBFD with MIMO.

REFERENCES

- [1] D. Bharadia, E. McMillin, and S. Katti, “Full duplex radios,” in *Proc. ACM SIGCOMM*, pp. 375–386, Aug. 2013.
- [2] S. Hong, J. Brand, J. Choi, M. Jain, J. Mehlman, S. Katti, and P. Levis, “Application of self-interference cancellation in 5G and beyond,” *IEEE Communication Magazine*, vol. 52, no. 2, pp. 114-121, Feb. 2014.
- [3] N. Reiskarimian, J. Zhou, and H. Krishnaswamy, “A CMOS passive LPTV non-magnetic circulator and its application in a full-duplex receiver,” *IEEE J. Solid-State Circuits*, vol. 52, no. 5, pp. 1358–1372, Mar. 2017.
- [4] D. Korpi, M. AghababaeTafreshi, M. Piilila, L. Anttila, and M. Valkama. “Advanced architectures for self-interference cancellation in full-duplex radios: Algorithms and measurements,” in *Proc. 50th Asilomar Conf. Signals, Systems and Computers*, pp. 1553–1557. Nov. 2016.
- [5] T. Chen, J. Zhou, N. Grimwood, R. Fogel, J. Marašević, H. Krishnaswamy, and G. Zussman, “Full-duplex wireless based on a small-form-factor analog self-interference canceller,” in *Proc. 17th ACM Int. Symp. Mobile Ad Hoc Networking and Computing*, pp. 357–358. Jul. 2016.

- [6] H. Hamazumi, K. Imamura, N. Iai, K. Shibuya, and M. Sasaki, “A study of a loop interference canceller for the relay stations in an SFN for digital terrestrial broadcasting,” in *Proc. IEEE Global Communications Conf.*, pp. 167–171. Nov. 2000.
- [7] B. Chun, E. Jeong, J. Joung, Y. Oh, and Y. H. Lee, “Pre-nulling for self-interference suppression in full-duplex relays,” in *Proc. Asia-Pacific Signal and Information Processing Assoc. Annu. Summit Conf.*, pp. 91–97, Oct. 2009.
- [8] H. Ju, E. Oh, and D. Hong, “Improving efficiency of resource usage in two-hop full duplex relay systems based on resource sharing and interference cancellation,” *IEEE Trans. Wireless Commun.*, vol. 8, no. 8, pp. 3933–3938, Aug. 2009.
- [9] L. Laughlin, M. A. Beach, K. A. Morris, and J. L. Haine, “Electrical balance duplexing for small form factor realization of in-band full duplex,” *IEEE Communication Mag.*, vol. 53, no. 5, pp. 102-110, May 2015.
- [10] L. Laughlin, C. Zhang, M. A. Beach, K. A. Morris, and J. Haine, “A widely tunable full duplex transceiver combining electrical balance

- isolation and active analog cancellation,” *IEEE Vehicular Techn. Conf.*, pp. 1-5, May 2015.
- [11] A. Kumar and S. Aniruddhan, “A 2.5-GHz CMOS Full-duplex front-end for asymmetric data networks,” *IEEE Trans. Circuits Syst. I, Reg. Papers*, vol. 65, no. 10, pp. 3174-3185, Oct. 2018.
- [12] A. E. Sayed, A. K. Mishra, A. H. Ahmed, A. H. M. Shirazi, S. Woo, Y. Choi, S. Mirabbasi, and S. Shekhar, “A Hilbert transform equalizer enabling 80 MHz RF self-interference cancellation for full-duplex receivers,” *IEEE Trans. Circuits Syst. I, Reg. Papers*, vol. 66, no. 3, pp. 1153-1165, Mar. 2019.
- [13] Z. Deng, H. J. Qian and X. Luo, “Tunable quasi-circulator based on a compact fully-reconfigurable 180 hybrid for full-duplex transceivers,” *IEEE Trans. Circuits Syst. I, Reg. Papers*, vol. 66, no. 8, pp. 2949-2962, Aug. 2019.
- [14] L. Zhang and H. Krishnaswamy, “Arbitrary analog/RF spatial filtering in digital MIMO receiver arrays,” *IEEE J. Solid-State Circuits*, vol. 52, no. 12, pp. 3392–3404, Dec. 2017.

- [15] T. Riihonen, S. Werner, and R. Wichman, "Mitigation of loopback self-interference in full-duplex MIMO relays," *IEEE Trans. Signal Process.*, vol. 59, no. 12, pp. 5983–5993, Dec. 2011.
- [16] K. M. Nasr, J. P. Cosmas, M. Bard, and J. Gledhill, "Performance of an echo canceller and channel estimator for on-channel repeaters in DVBT/H networks," *IEEE Trans. Broadcast.*, vol. 53, pp. 609–618, Sept. 2007.
- [17] T. Riihonen, S. Werner, and R. Wichman, "Transmit power optimization for multiantenna decode-and-forward relays with loopback self-interference from full-duplex operation," in *Proc. Asilomar Conf. Signals, Systems and Computers (ACSSC)*, pp. 1408–1412, 2011.
- [18] B. Chun and H. Park, "A spatial-domain joint-nulling method of self-interference in full duplex relays," *IEEE Commun. Lett.*, vol. 16, no. 4, pp. 436–438, 2012.
- [19] J. I. Choi, M. Jain, K. Srinivasan, P. Levis, and S. Katti, "Achieving single channel, full duplex wireless communication," in *Proc. Annu. Int. Conf. Mobile Computing and Networking (MobiCom)*, pp. 1–12, 2010.
- [20] N. Singh, D. Gunawardena, A. Proutiere, B. Radunovic, H. V. Balan, and

- P. B. Key, “Efficient and fair MAC for wireless networks with selfinterference cancellation,” in Proc. 9th Int. Symp. *Modeling and Optimization in Mobile, Ad Hoc and Wireless Networks*, pp. 94–101, 2011.
- [21] S. H. Li and R. D. Murch, “Full-duplex wireless communication using transmitter output based echo cancellation,” in Proc. *IEEE Global Commun. Conf. (GLOBECOM)*, pp. 1–5, 2011.
- [22] W. Cheng, X. Zhang, and H. Zhang, “Imperfect full duplex spectrum sensing in cognitive radio networks,” in Proc. *3rd ACM Workshop Cognitive Radio Networks*, pp. 1–6, 2011.
- [23] J. Zhang, O. Taghizadeh, and M. Haardt, “Transmit strategies for full-duplex point-to-point systems with residual self-interference,” in Proc. *Int. ITG Workshop Smart Antennas (WSA)*, pp. 1–8, 2013.
- [24] W. Afifi and M. Krunz, “Exploiting self-interference suppression for improved spectrum awareness/efficiency in cognitive radio systems,” in Proc. *IEEE INFOCOM Conf.*, pp. 1258–1266, 2013.
- [25] S. P. Herath and T. Le-Ngoc, “Sum-rate performance and impact of self-interference cancellation on full-duplex wireless systems,” in Proc. *IEEE Int. Symp. Personal Indoor and Mobile Radio Communications (PIMRC)*,

pp. 881–885, 2013.

- [26] S. Johnston and P. Fiore, “Full-duplex communications via adaptive nulling,” in *Proc. Asilomar Conf. Signals, Systems and Computers (ACSSC)*, pp. 1628–1631, 2013.
- [27] B. Kaufman, J. Lilleberg, and B. Aazhang, “An analog baseband approach for designing full duplex radio,” in *Proc. Asilomar Conf. Signals, Systems and Computers (ACSSC)*, pp. 987–991, 2013.
- [28] Y.-S. Choi and H. Shirani-Mehr, “Simultaneous transmission and reception: Algorithm, design and system level performance,” *IEEE Trans. Wireless Commun.*, vol. 12, no. 12, 2013.
- [29] M. Zhou, H. Cui, L. Song, and B. Jiao, “Transmit-receive antenna pair selection in full duplex systems,” *IEEE Wireless Commun. Lett.*, vol. 3, no. 1, pp. 34–37, 2014.
- [30] S. Goyal, P. Liu, S. Panwar, R. DiFazio, R. Yang, J. Li, and E. Bala, “Improving small cell capacity with common-carrier full-duplex radios,” in *Proc. IEEE Int. Conf. Communications (ICC)*, pp. 4987–4993, 2014.
- [31] S. H. Li and R. D. Murch, “An investigation into baseband techniques for single-channel full-duplex wireless communication systems,” *IEEE Trans.*

- Wireless Commun.*, vol. 13, no. 9, pp. 4794–4806, 2014.
- [32] W. Li, J. Lilleberg, and K. Rikkinen, “On rate region analysis of half- and full-duplex OFDM communication links,” *IEEE J. Sel. Areas Commun.*, vol. 32, no. 9, pp. 1688–1698, 2014.
- [33] D. Nguyen, L. Tran, P. Pirinen, and M. Latva-aho, “On the spectral efficiency of full-duplex small-cell wireless systems,” *IEEE Trans. Wireless Commun.*, vol. 13, no. 9, pp. 4896–4910, 2014.
- [34] D. Korpi, L. Anttila, V. Syrjälä, and M. Valkama, “Widely linear digital self-interference cancellation in direct-conversion full-duplex transceiver,” *IEEE J. Sel. Areas Commun.*, vol. 32, no. 9, pp. 1674–1687, 2014.
- [35] P. Lioliou, M. Viberg, M. Coldrey, and F. Athley, “Self-interference suppression in full-duplex MIMO relays,” in *Proc. Asilomar Conf. Signals, Systems and Computers (ACSSC)*, pp. 658–662, 2010.
- [36] T. Riihonen, S. Werner, and R. Wichman, “Residual self-interference in full-duplex MIMO relays after null-space projection and cancelation,” in *Proc. Asilomar Conf. Signals, Systems and Computers (ACSSC)*, pp. 653–657, 2010.

- [37] Y. Hua, “An overview of beamforming and power allocation for MIMO relays,” in *Proc. IEEE Military Communications Conf.*, pp. 375–380, 2010.
- [38] B. P. Day, A. R. Margetts, D. W. Bliss, and P. Schniter, “Full-duplex bidirectional MIMO: Achievable rates under limited dynamic range,” *IEEE Trans. Signal Process.*, vol. 60, no. 7, pp. 3702–3713, 2012.
- [39] T. M. Kim, H. J. Yang, and A. Paulraj, “Distributed sum-rate optimization for full-duplex MIMO system under limited dynamic range,” *IEEE Signal Process. Lett.*, vol. 20, no. 6, pp. 555–558, 2013.
- [40] D. Nguyen, L.-N. Tran, P. Pirinen, and M. Latva-aho, “Precoding for full duplex multiuser MIMO systems: Spectral and energy efficiency maximization,” *IEEE Trans. Signal Process.*, vol. 61, no. 16, pp. 4038–4050, 2013.
- [41] M. Vehkaperä, T. Riihonen, and R. Wichman, “Asymptotic analysis of full-duplex bidirectional MIMO link with transmitter noise,” in *Proc. IEEE Int. Symp. Personal Indoor and Mobile Radio Communications*, pp. 1265–1270, 2013.
- [42] A. C. Cirik, R. Wang, and Y. Hua, “Weighted-sum-rate maximization for

- bi-directional full-duplex MIMO systems,” in *Proc. Asilomar Conf. Signals, Systems and Computers (ACSSC)*, pp. 1632–1636, 2013.
- [43] S. Huberman and T. Le-Ngoc, “Sequential convex programming for full-duplex single-user MIMO systems,” in *Proc. IEEE Int. Conf. Communications (ICC)*, pp. 5078–5082, 2014.
- [44] S. Li, R. Murch, and V. Lau, “Linear transceiver design for full-duplex multi-user MIMO system,” in *Proc. IEEE Int. Conf. Communications (ICC)*, pp. 4921–4926, 2014.
- [45] A. C. Cirik, R. Wang, Y. Rong, and Y. Hua, “MSE-based transceiver designs for bi-directional full-duplex MIMO systems,” in *Proc. 15th IEEE Workshop Signal Processing Advances in Wireless Communications (SPAWC)*, pp. 384–388, 2014.
- [46] A. C. Cirik, Y. Rong, and Y. Hua, “Achievable rates and QoS considerations of full-duplex MIMO radios for fast fading channels with imperfect channel estimation,” *IEEE Trans. Signal Process.*, vol. 62, no. 15, pp. 3874–3886, 2014.
- [47] D. Korpi, L. Anttila, and M. Valkama, “Reference receiver-based digital self-interference cancellation in MIMO full-duplex transceivers,” in *Proc.*

- Globecom Workshop—Broadband Wireless Access*, pp. 1001–1007, 2014.
- [48] A. C. Cirik, R. Wang, Y. Hua, and M. Latva-aho, “Weighted sumrate maximization for full-duplex MIMO interference channels,” *IEEE Trans. Commun.*, vol. 63, no. 3, pp. 801–815, 2015.
- [49] K. Lin, R. H. Messerian, and Y. Wang, “A digital leakage cancellation scheme for monostatic FMCW radar,” in *Proc. IEEE MTT-S Int. Microwave Symp. Dig.*, pp. 747–750, 2004.
- [50] K. Lin, Y. E. Wang, C.-K. Pao, and Y.-C. Shih, “A Ka-band FMCW radar front-end with adaptive leakage cancellation,” *IEEE Trans. Microw. Theory Techn.*, vol. 54, no. 12, pp. 4041–4048, 2006.
- [51] H. Nawaz and I. Tekin, “Dual-polarized, differential fed microstrip patch antennas with very high interport isolation for full duplex communication,” *IEEE Trans. Antennas Propagation*, vol. 65, no. 12, pp. 7355–7360, Oct. 2017.
- [52] T. Dinc and H. Krishnaswamy. “A T/R antenna pair with polarization-based reconfigurable wideband self-interference cancellation for simultaneous transmit and receive,” *Proc. IEEE International Microwave Symposium*, pp. 1–4, Jul. 2015.

- [53] B. Debaillie, D. V. D. Broek, C. Lavín, B. V. Liempd, E. A. M. Klumperink, C. Palacios, J. Craninckx, B. Nauta, and A. Pärssinen “Analog/RF solutions enabling compact full duplex radios,” *IEEE Journal of Selected Areas in Communication*, vol. 32, no. 9, pp. 1662-1672, Jun. 2014.
- [54] M. E. Knox, “Single antenna full duplex communications using a common carrier,” in *Proc. IEEE Wireless & Microwave Technology Conf.*, pp. 1-6, Apr. 2012.
- [55] M. Jain, J. Choi, T. Kim, D. Bharadia, K. Srinivasan, S. Seth, P. Levis, S. Katti, and P. Sinha, “Practical, real-time, full duplex wireless,” in *Proc. 17th Annu. Int. Conf. Mobile Computer Network*, pp. 301–312, Sep. 2011.
- [56] L. Laughlin, M. A. Beach, K. A. Morris, and J. L. Haine, “Optimum single antenna full duplex using hybrid junctions,” *IEEE Journal on Selected Areas in Communications*, vol. 32, no. 9, pp. 1653-1661, Jun. 2014.
- [57] A. Tang and X. Wang, “Balanced RF-circuit based self-interference cancellation for full duplex communications,” *Journal Ad Hoc Networks*, vol. 24, Part A, pp. 214-227, Jan. 2015.

- [58] H. son, H. Park, H. Jeon, “ Design of a circularly polarized radio-frequency identification reader antenna with high return loss,” *IET microwaves, antennas and propagation*, vol. 5, no. 15, pp. 1844-1848, Aug. 2011
- [59] Y. Jeong, D. Ahn, C. Kim, and I. Chang, “A feed-forward amplifier using an equal group-delay signal cancellation technique,” *Microwave Journal*, vol. 50, no. 4, pp. 126-132. Apr. 2007.
- [60] S. Lucyszyn and I. D. Robertson, “Analog reflection topology building blocks for adaptive microwave signal processing applications,” *IEEE Microwave Theory Tech.*, vol. 43, no. 3, pp. 601–611, Mar. 1995.
- [61] Q. Wang, H. Kang, S. Jeong, J. Jeong, P. Kim, and Y. Jeong, “Analysis and design of conventional wideband branch line balun,” *International Symposium on Information Technology Convergence*, pp. 386-389, Oct. 2015

요 약

차세대 무선통신을 위한 동일대역 전이중통신 무선 전단부

이 논문은 RF 무선 전단부에서 60 dB 송수신기의 격리특성을 얻기 위한 자기간섭 상쇄 (self-interference cancellation) 기술의 수학적 분석과 광대역 60 dB 격리특성을 얻기 위한 새로운 구조의 동일대역 전이중 무선 통신 전단부 회로를 제안한다.

동일대역 전이중 무선 통신은 기존의 TDD 및 FDD 시스템과 비교해 무선통신 시스템의 데이터 전송 효율을 증가시킬 수 있는 기술이다. 하지만 같은 주파수 대역과 시간에서 송신과 수신이 이루어지기 때문에 이를 분리하기 위해 자기간섭 상쇄 기술이 필요하다. 송수신기의 특성과 고조파 및 노이즈에 따른 자기간섭 상쇄 기술의 기준이 다르므로 이를 분류하고 특성을 제시한다.

수학적 분석에서는 신호의 조건에 따른 자기간섭 상쇄기술의 특성을 제시한다. 자기간섭 상쇄 기술은 결국 두 개의 신호가 서로 상쇄되는 것이다. 따라서 두 신호의 크기와 위상 및 군지연 차이에 따른 상쇄 정도와 주파수 대역폭에 관한 분석을 제시한다. 이를 바탕으로 광대역 송수신 격리특성을 얻기 위한 두 신호의 크기와 위상 차이 및 군지연의 범위를 제시한다.

수학적 분석을 바탕으로 서큘레이터를 이용한 광대역 동일대역 전이중 무선통신 전단부를 제시한다. 자기 장치인 서큘레이터는

고주파에서는 특성이 열화되는 단점이 있지만 자기간섭 제거 기술을 사용하여 쉽게 60dB 송수신 분리특성을 얻을 수 있다. 따라서, 60 dB 격리 대역폭을 향상시키기 위해 2 개의 서큘레이터를 사용하는 새로운 구조를 제안했다. 제안하는 구조와 높은 반사 특성을 갖는 안테나를 이용한 시뮬레이션 및 측정 결과를 제시한다.

또한 앞서 말한 자기 장치의 단점을 극복한 동일대역 전이중 무선통신 전단부 역시 제안한다. 이 구조는 송수신부의 광대역 격리 특성을 구현하기 위해 180° 위상차를 갖는 평형 전력 분배기와 물리적 균형구조를 사용했다. 4 개의 다이폴 안테나를 사용해 안테나의 배열에 따른 방사 특성과, 안테나 사이의 거리에 따른 동일대역 전이중 무선통신 전단부의 송수신 격리 특성을 제시한다.

키워드 : 균형구조, 동일대역, 서큘레이터, 자기간섭제거, 전이중 통신, 평형 전력 분배기, 페라이트

CURRICULUM VITAE

Junhyung Jeong

#7304, Division of Electronics and Information Engineering, Chonbuk National University,
567 Baeje-daero, Jeonju-si, Chollabuk-do, 561-756, Republic of Korea

Mobile Phone : +82-10-9485-5827

E-mail: jjunh05@jbnu.ac.kr , jjunh05@gmail.com

RESEARCH INTERESTS

RF passive/active circuits design such as **matching network, impedance transformer, power amplifier and MMIC amplifier.**

EDUCATIONS

Ph.D., Electronic and Information Engineering, <i>Jeonbuk National University, Republic of Korea</i> Academic Advisor : Professor Yongchae Jeong	2014-present
--	--------------

M.E., Electronic and Information Engineering, <i>Jeonbuk National University, Republic of Korea</i> Academic Advisor : Professor Yongchae Jeong	2012-2014
---	-----------

B.E., Electronic Engineering, <i>Jeonbuk National University, Republic of Korea</i>	2006-2012
--	-----------

AWARDS AND HONORS

International Symposium on Information Technology Convergence Certificate of Excellent Oral Presentation with “RF energy harvesting circuit for low power applications”	2016
Outstanding graduate student award In recognition of contribution to the principles of graduate research while in pursuit of the Doctoral degree in Division of Electronics and Information Engineering	2018
2018 Asia-Pasific Microwave Conference Student and Young Engineer Design Competitions Student and Young Engineer Design Competitions Second prize	2018

REFERENCES

Yongchae Jeong, Ph.D

Professor, Academic Advisor (*Senior Member, IEEE*)

#7304, Division of Electronics and Information Engineering,

Chonbuk National University,

567 Baekje-daero, Jeonju-si, Chollabuk-do, 54896, Republic of Korea

Phone : +82-63-270-2458

Fax : +82-63-270-2394

E-mail : ycjeong@jbnu.ac.kr

PUBLICATIONS

INTERNATIONAL PEER-REVIEWED JOURNALS

- [1] **Junhyung Jeong**, Girdhari Chaudhary, Yongchae Jeong, “Time mismatch effect in linearity of hybrid envelope tracking power amplifier,” *IEEE Microwave Wireless Compon. Letter*, vol. 25, no. 8, pp. 550-552, Aug. 2015.

- [2] **Junhyung Jeong**, Phirun Kim, Yongchae Jeong, “High efficiency power amplifier with frequency band selective matching networks,” *Microwave Optic. Techno. Lett.*, vol. 57, no. 9, pp. 2031-2034, Sep. 2015.

- [3] **Junhyung Jeong**, and Yongchae Jeong, “A novel dual-band RF energy harvesting circuit with power management unit for low power,” *Microwave Optic. Techno. Lett.*, vol. 59, no. 5, pp. 1808-1812, May 2017.

- [4] Seungho Jeong, **Junhyung Jeong**, Yongchae Jeong, “A design of a impedance tuner with programmable characteristic for RF amplifiers,” *IEEE Microwave Wireless Compon. Letter*, vol. 27, no. 5, pp. 473-475, May 2017.

- [5] Girdhari Chaudhary, **Junhyung Jeong**, Yongchae Jeong, “Differential fed antenna with high self-interference cancellation for in-band full-duplex communication system,” *IEEE ACCESS*, vol. 7, pp. 45340-45348, Mar. 2019.
- [6] Girdhari Chaudhary, **Junhyung Jeong**, Qi Wang, Yongchae Jeong, “A design of source-degenerated CMOS active negative group delay circuit using bonding wire,” *IEICE Electronics Express*, vol. 16, no. 7, pp. 1 -5, Apr. 2019.
- [7] **Junhyung Jeong**, Girdhari Chaudhary, Yongchae Jeong, “Efficiency enhancement of cross cancellation power amplifier using negative group delay circuit,” *Microwave Optic. Techno. Lett.*, vol. 61, no. 7, pp. 1673-1677, Jul. 2019.
- [8] **Junhyung Jeong**, Phanam Pech, Yongchae Jeong and Sangmin Lee, “Wafer-level-packaged X-band internally matched power amplifier using silicon interposer technology,” *IEEE Microwave Wireless Compon. Letter*, vol. 29, no. 10, pp. 445-447, Oct. 2019.
- [9] Girdhari Chaudhary, **Junhyung Jeong**, Yongchae Jeong, “Microstrip antenna with high self-interference cancellation using phase

reconfigurable feeding network for in-band full duplex,” *Microwave Optic. Techno. Lett.*, DOI: 10.1002/mop (early access).

DOMESTIC JOURNALS

- [1] Girdhari Chaudhary, **Junhyung Jeong**, Phirun Kim, Yongchae Jeong, “Negative Group Delay Circuit with Improved Signal Attenuation and Multiple Pole Characteristics,” *Journal of Electromagnetic Engineering and Science*, vol. 15, no. 2, pp. 76-81, Apr. 2015.
- [2] Phirun Kim, Junsik Park, **Junhyung Jeong**, Seungho Jeong, Girdhari Chaudhary, and Yongchae Jeong, “High Selectivity Coupled Line Impedance Transformer with Second Harmonic Suppression,” *Journal of Electromagnetic Engineering and Science*, vol. 16, no. 1, pp. 13-18, Jan. 2016.

INTERNATIONAL CONFERENCE PRESENTATIONS

- [1] Jongsik Lim, **Junhyung Jeong**, Phirun Kim, Yongchae Jeong, Sang-Min Han, and Dal Ahn, “4-way power divider using common DGS and stacked-substrate structure,” *Progress in Electromag. Research Sympos.*, pp. 934, Aug. 2014.
- [2] **Junhyung Jeong**, Seungwook Lee, Girdhari Chaudhary, and Yongchae, “Tunable negative group delay circuit with improved signal attenuation,” *International Symposium on Information Technology Convergence*, vol. 3, no. 2, pp. 55-56, Oct. 2014.
- [3] Junsik Park, Jaeyeon Kim, **Junhyung Jeong**, and Yongchae, " CMOS RF energy harvesting rectifier using body bias feedback technique," *International Symposium on Information Technology Convergence*, vol. 3, no. 2, pp. 561-562, Oct. 2014.
- [4] Girdhari Chaudhary, Phirun Kim, **Junhyung Jeong**, Yongchae Jeong, Jongsik Lim, “dual-band negative group delay circuit using dDefected microstrip structure,” *IEEE Radio & Wireless Week*, pp. 129-131, Jan. 2015.
- [5] Phirun Kim, **Junhyung Jeong**, Girdhari Chaudhary, Yongchae Jeong, and Jongsik Lim, “Bandpass-to-allstop switchable filter with broadband

- harmonics suppression,” *Progress in Electromag. Research Sympos.*, pp. 1755, Jul. 2015.
- [6] Phirun Kim, **Junhyung Jeong**, Girdhari Chaudhary, and Yongchae Jeong, “A design of unequal termination impedance power divider with filtering and out-of-band suppression characteristics,” *European Microwave Conf.*, pp. 123-126, Sep. 2015.
- [7] Qi Wang, **Junhyung Jeong**, Phirun Kim, and Yongchae Jeong, “Analysis and design of conventional wideband branch line balun,” *International Symposium on Information Technology Convergence*, pp. 386-389, Oct. 2015.
- [8] Girdhari Chaudhary, Phirun Kim, **Junhyung Jeong**, Yongchae Jeong, Jongsik Lim, “Power divider with tunable positive and negative group delays using parasitic compensated PIN diode,” 2016 *Radio and Wireless Symposium*, pp. 4-6, Jan. 2016.
- [9] Girdhari Chaudhary, Phirun Kim, **Junhyung Jeong**, Yongchae Jeong, Jongsik Lim, “A design of negative group delay power divider: coupling matrix approach with finite unloaded-Q resonators,” 2016 *IEEE International Microwave Symposium*, May 2016.

- [10] Jageon Koo, Seungwook Lee, **Junhyung Jeong**, Girdhari Chaudhary, and Yongchae Jeongs, “Low noise figure CMOS 2-port active inductor using LC resonator,” *Progress in Electromag. Research Sympos.*, pp. 3222, Aug. 2016.
- [11] Girdhari Chaudhary, Phirun Kim, **Junhyung Jeong**, and Yongchae Jeong, “A power divider with positive and negative group delay characteristics,” 2016 *URSI Asia-Pacific Radio Science Conf.*, pp. 1195-1197, Aug. 2016.
- [12] **Junhyung Jeong**, Phirun Kim, Yongchae Jeong and Jongsik Lim, “RF energy harvesting circuit for low power applications,” *International Symposium on Information Technology Convergence*, pp. 96-97, Oct. 2016.
- [13] **Junhyung Jeong**, Jageon Koo, and Yongchae Jeong, “X -band GaN power amplifier using interposer-based MMIC,” *Progress in Electromag. Research Sympos.*, pp. 1825, May 2017.
- [14] Jageon Koo, **Junhyung Jeong**, and Yongchae, “A fully integrated variable gain amplifier for X -band application,” *Progress in Electromag. Research Sympos.*, pp. 1824, May 2017.

- [15] **Junhyung Jeong**, Phirun Kim, Yongchae Jeong and Jongsik Lim, “Harmonics suppressed band-pass matching network for high efficiency power amplifier,” ” *European Microwave Conf.*, pp. 280-283, Oct. 2017
- [16] Boram An, **Junhyung Jeong**, Girdhari Chaudhary, Seok-Hawn Park, Ji-Hoon Lee, and Yongchae Jeong, “A design of tunable phase shifter using capacitive termination,” *International Symposium on Information Technology Convergence*, pp. 184-186, Oct. 2017.
- [17] **Junhyung Jeong**, Phirun Kim, Phanam Pech, Yongchae Jeong and Sangmin Lee, “Quasi-MMIC high power amplifier with silicon IPD matching network,” *European Microwave Conf.*, pp. 340-343, Sep. 2018
- [18] **Junhyung Jeong**, Phanam Pech, Qi Wang, Yongchae Jeong, and Sangmin Lee, “A study of matching network for X-band MMIC high power amplifier,” *International Symposium on Information Technology Convergence*, pp. 423-425, Oct. 2018.
- [19] Phanam Pech, **Junhyung Jeong**, Girdhari Chaudhary, and Yongchae Jeong, “Wideband negative group delay circuit using 180° hybrid and in-phase power combiner,” *International Symposium on Information Technology Convergence*, pp. 309-311, Oct. 2018.

- [20] Girdhari Chaudhary, **Junhyung Jeong**, Phanam Pech, Phirun Kim, and Yongchae Jeong, “Arbitrary prescribed wideband flat group delay circuit for self-interference cancellation circuits,” in *Proc. Asia- Pacific Microwave Conf.*, Nov. 2018
- [21] **Junhyung Jeong**, Phirun Kim, Phanam Pech, Yongchae Jeong and Sangmin Lee, “Substrate-integrated waveguide impedance matching network with bandpass filtering,” 2016 *Radio and Wireless Symposium*, Jan. 2019.
- [22] **Junhyung Jeong**, Girdhari Chaudhary, Phanam Pech, Dongshin Kim, and Yongchae Jeong, “A return loss equalizer using non-reciprocal device for in-band full-duplex RF front-end,” *Europe-Korea Conf. on Science and Technology*, Jul. 2019.
- [23] Girdhari Chaudhary, **Junhyung Jeong**, Phanam Pech, Phirun Kim, and Yongchae Jeong, “High Self-Interference Cancellation Antenna for In-Band Full Duplex Communication System,” *European Microwave Conf.*, pp. 236-239, Oct. 2019
- [24] Phirun Kim, Qi Wang, Phanam Pech, **Junhyung Jeong**, and Yongchae Jeong, “Compact square/triangle mixed-shape quarter-mode substrate

integrated waveguide bandpass filter with wide stopband,” *European Microwave Conf.*, pp. 448-451, Oct. 2019

